NTNU – Trondheim
Norwegian University of
Science and Technology

IPR Modeling for Coning Wells

Wynda Astutik

Petroleum Engineering
Submission date: August 2012
Supervisor: Curtis Hays Whitson, IPT

Norwegian University of Science and Technology
Department of Petroleum Engineering and Applied Geophysics

Wynda Astutik

IPR Modeling for Coning Wells

Thesis for the degree of Master of Science

Trondheim
August 12, 2012

Norwegian University of Science and Technology
Faculty of Engineering Science and Technology
Department of Petroleum Engineering and Applied Geophysics

NTNU
Norwegian University of
Science and Technology

Abstract

In this study, based on the work of Vogel, we generated the Inflow Performance Relationship (IPR) curves and its dimensionless form at any stage of depletion using black-oil simulator results. The IPR was generated for horizontal well with gas and water coning problems, producing from thin oil reservoir sandwiched between gas cap and aquifer. Two empirical IPR equations adopted from SPE paper by Whitson was also presented here. The first empirical relationship was developed based on simulated data for each reservoir pressure (stage of depletion) while the second relationship was developed based on all generated data.

A fully implicit black-oil Cartesian model with total grid number of 1480 and 150 ft total thickness was used as reservoir model. The horizontal well extends through the full length of reservoir in y-direction with only one grid number along the horizontal section which makes the model a 2D problem. Sensor reservoir simulator and Pipe-It software were utilized to generate the IPR data.

This work also includes a sensitivity study to understand the effect of several parameters to gas and water coning behavior, well placement optimization, coning collapse study, and the effect of coning to maximum well production rate. In coning collapse study, a relationship between flowing bottom-hole pressure and reservoir pressure when the cone collapse is provided in graphical form. This could be useful in field application where chocking the well to lower flowing bottom-hole pressure has become one alternative to reduce coning problems.

Acknowledgements

First and foremost I offer my sincerest gratitude to my supervisor Professor Curtis H. Whitson for his excellent guidance, caring, and support not only thought this work but also throughout my Master study. His research ideas, time, interesting discussion, and encouragement, made it possible for me to complete this thesis. One could not wish for a better or friendlier supervisor.

I acknowledge Petrostreamz a/s for the Pipe-It license and Coats Engineering, Inc. for the Sensor license.

I would like to thank Faizul Hoda from Petrostreamz a/s for his technical support in Pipe-It application and VBS scripting. And Snjezana Sunjerga from PERA, not only for valuable technical discussion, but also for her encouragement, supports, and care–thank you for being my sister far away from home.

It is a great pleasure to thank everyone who supports me during my master study: Paula, my best friend at IPT who made this 2 years master degree becomes memorable; Indonesian communities in Trondheim that make me feel like home during my stay in Trondheim; and Arif Kuntadi family, who always there to help with an open arms.

I am truly indebted and thankful to my lovely Mom, Asmanik, for her support through endless prays and weekly calls. And finally, I owe sincere and earnest thankfulness to my beloved family. My husband, Agus Ismail Hasan, for his unconditional love, patience, and support; and my little daughter, Aisyah, who always cheer me up with her total-cuteness. I dedicate this work for both of you.

Wynda Astutik

Table of Contents

List of Tables

List of Figures

Chapter 1

INTRODUCTION

1.1 Background

Horizontal well have become a popular option for oil production in petroleum industry. This type of well could accelerate oil production, control coning, and in some cases could turn uneconomical reserves into a commercial one (i.e. in low permeability reservoir, reservoir with viscous oil, thin reservoir, etc.). Thin reservoir is a very good candidate for horizontal well since the increases in formation thickness decrease the productivity ratio of the horizontal well to vertical well [13].

In reservoir with thin oil column, sandwiched between big gas cap and aquifer, gas and water coning most likely will occurs during oil production. Since the critical rates usually very low (and un-economic), the well usually produce at rate higher than the critical rates. This makes coning problems un-avoidable. In this condition, a three-phase flow (gas-oil-water) exists in production stream.

Inflow performance in a horizontal well could be estimate using an analytical solution or empirical IPR. The analytical solutions are based on single-phase flow principles and may not be appropriate for three-phase, gas-oil-water flow. Thus, an empirical IPR solution might be preferable. As author knowledge, there have not been any publications presenting IPR model for horizontal well with gas and water coning problem. The main objective of this study is to address this gap by developing an IPR model for horizontal well producing from thin oil reservoir underlying gas cap and overlaying aquifer, with gas and water coning problem.

1.2 Study Objectives

The main objective of this study was to develop Inflow Performance Relationship (IPR) for horizontal well producing from oil reservoir with gas and water coning problem. Both dimensional and dimensionless IPR with its best-fit equations were presented in this study.

The other objectives are to conduct a sensitivity study to understand the effect of several parameters to gas and water coning behavior and to do well placement optimization and coning collapse study.

1.3 Description of Employed Software

1.3.1 Sensor

Sensor, which is stands for System for Efficient Numerical Simulation of Oil Recovery, is the compositional and black oil reservoir simulation software that was developed by Coats Engineering, Inc. *This software is a generalized 3D numerical model used by engineers to optimize oil and gas recovery processes through simulation of compositional and black oil fluid flow in single porosity, dual porosity, and dual permeability petroleum reservoir* [1].

This numerical simulation was used to run the model and extract all values needed to generate IPR curves. Sensor was also used to study the gas and water coning behavior and how it is affect production performance.

1.3.2 Pipe-It

Pipe-It is a unique application generated by Petrostreamz, a software company developed at PERA AS. This software allows the user to graphically and computationally integrate models and optimize petroleum assets [2]. Pipe-It can chains several applications in series and parallel and launch any software on any operating system.

In this study, Pipe-It is used to simplify the Sensor run. MapLinkz and Linkz applications inside Pipe-It were also used in extracting data from simulation output, thus avoiding lots of manual copy and paste work that can be time consuming.

Chapter 2

MODEL INITIALIZATION

2.1 Data Acquisition and Preparation

One objective in this study is to observe gas and water coning behavior in a reservoir with horizontal well producing from thin oil zone sandwiched between big gas cap and aquifer. A further IPR curves will also be constructed for this certain reservoir. Thus, a base case model that represents this condition need to be generated.

For reference, we use the three-well Sensor compositional model that was generated by Dr. Alexander Juell. This reference model contains rock and fluid properties which are similar to Troll field; a natural gas an oil field in North sea that has thin oil rims between large gas cap and active aquifer. Several modifications were made on this reference model to generate the base case, this which the intention to have reservoir model that suit the objectives of the project.

The reference model is a fully implicit 3D Cartesian model with 3278 ft, 3280 ft, and 160 ft; total length in x, y, and z-direction respectively. This model use total number of grid of 1480 ($N_x = 40$, $N_y = 1$, $N_z = 37$). The horizontal well extends through the full length of reservoir in y-direction with only one grid number along the horizontal section, this make the model become 2D problems with uniform pressure (influx) along the well.

Table 2.1: Comparison between Compositional and Black Oil Run.

Dataset	CPU	Reservoir Volume			Surface Volume		
		Water	Oil	Gas	Water	Oil	Gas
	sec.	MRB	MRB	MRB	MSTB	MSTB	MMCF
Sensor EOS	285.29	594269	15289	1435906	592048	14620	1256481
Sensor BO	20.5	594269	15289	1435906	592048	14261	1256637

2.2 Conversion from Compositional Model to Black Oil Model

In general, for the same dataset, compositional model have higher CPU time compare to black oil model. With implicit run, the ratio between compositional CPU times with black oil could be very high [3]. This due to higher number of equations per grid blocks that need to be solved in compositional model.

Having a model with shorter simulation is more preferable, especially when the CPU time is high. In this study, conversion from compositional to black oil model was done to have shorter CPU time. BLACKOIL options in Sensor simulator make it possible to do it automatically. This option makes running a model either in compositional mode or black oil mode easier. *With this option, Sensor using Whitson and Torp method* [34] *to internally generate the black oil pvt table from the PV-TEOS data, and then uses the black oil table for pvt properties rather than the eos* [3]. In our dataset, additional INJECTION GAS EQUILIBRIUM keyword is used to obtain better agreement between black oil and compositional run. Using this keyword, the saturation pressures in black oil table are elevated above the original saturation pressure by adding increments of injection bubble point equilibrium gas.

Table 2.1 summarizes the comparison between compositional and black oil run. Black oil has CPU time almost 10 times lower than compositional run, which is quiet significant reduction. The initial fluids in place (reservoir condition) results between both runs are the same. The surface volume for oil and gas between both runs is slightly different due to differences in B_g and B_o from both runs.

Fig. 2.1 and **Fig. 2.2** present the gas oil ratio and water comparison between both compositional and black oil runs. Sensor black oil (Sensor BO) produces higher GOR than Sensor compositional (Sensor EOS) in range of 5% error. The water cut is also different in range of 5% error. The oil rate and average reservoir pressure between them are on-top of each other.

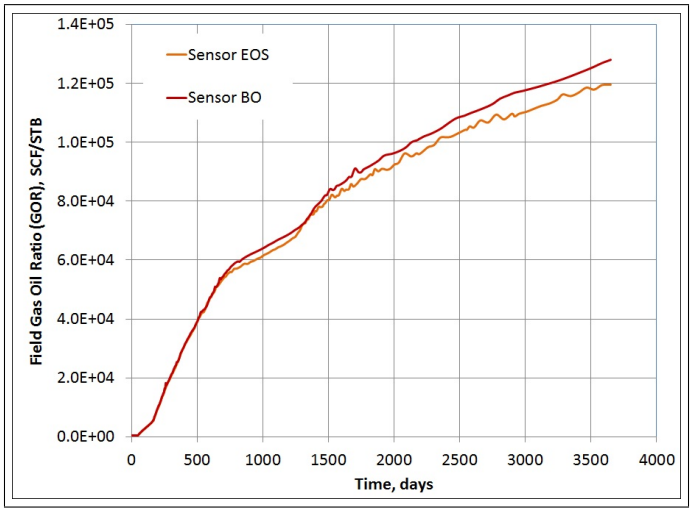

Figure 2.1: GOR comparison between compositional and black oil run.

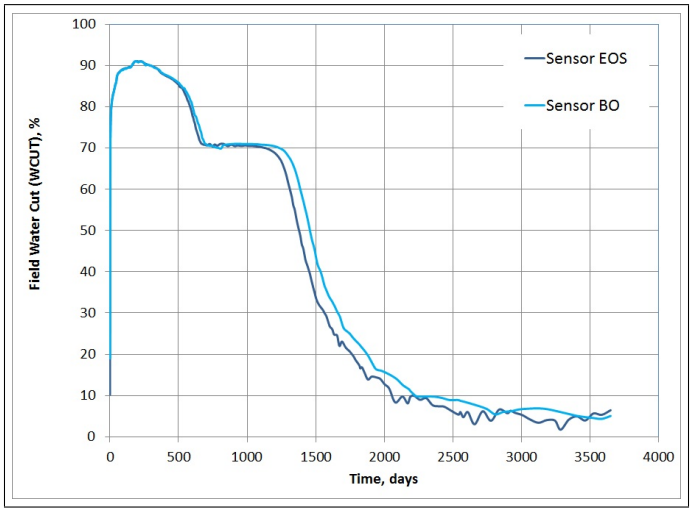

Figure 2.2: Water cut comparison between compositional and black oil run.

In black-oil model, mass transfer between phases is represented by solution gas-oil ratio (R_s) and the compressibility effect (Formation Volume Factor). These assumptions on fluid properties are used to eliminate the need for equation of state (EOS) and phase equilibrium calculation, which can take up to 70% of the total simulation time ([8, 21]). By using black oil model in this study, a high amount of simulation time could be saved. It is also proved in validation process that black

oil model, with a shorter run time, will able to presents the same simulation results as compositional model (in range of 5% error).

2.3 Grid Sensitivity

One of the basics of reservoir simulation is the finite-difference formulation where the spatial segmentation of the reservoir model is discretized into grid blocks. Since the discretization error proportional to Δx^2, the smaller the grid blocks used, the smaller will be the error involved. For the same area or volume, the smaller the grid blocks, more number of grids we need to use. And unfortunately, the computing time increase with the number of grids in the model. Thus, it is important to have optimum grids number and distribution so that the model could representative enough to meet the study objectives with the reasonable computing time.

Grid sensitivity study was done to find the optimum number of grid in x and z-direction, while number of grid in y-direction is set to be one (along the horizontal well). An excel file with the solver utilization was used in grid generation process. The gridding method for x and z-direction is:

$$\mathbf{x-direction}: \quad \Delta x_i = \Delta x_w \times R_x^i, \qquad i = 1, 2, \cdots, N_x \tag{2.1}$$

$$\mathbf{z-direction}: \quad \Delta z_k = \Delta z_w \times R_z^k, \qquad k = 1, 2, \cdots, N_z \tag{2.2}$$

Where Δx_i and Δz_i is the grid size in block-i (after the well grid) in x-direction and z-direction, respectively; Δx_w and Δz_w are the well-grid sizes in x and z-direction; N_x and N_z are the total numbers of grid in x and z-direction; R_x defined as $\Delta x_{i+1}/\Delta x_i$ and R_z defined as $\Delta z_{i+1}/\Delta z_i$. By using this gridding method, the grid blocks are finer near the wellbore and become larger with increasing distance from the well. This type of gridding is preferable since the flow properties are expected to change rapidly near the well; the coning behavior is also best studied in detail with this type of gridding.

2.3.1 Nx Sensitivity

Because of symmetrical geometric, a half well model simulation will be sufficient. The well is located in left boundary of the model ($i = 1$) with horizontal section along the y-direction. Perforation point is located 95 ft from the top of reservoir.

In N_x sensitivity, the Sensor simulation was run with $N_z = 25$ and $N_y = 1$, while the N_x value is vary from $20 - 45$. The simulation results are then compared to find the converged solution.

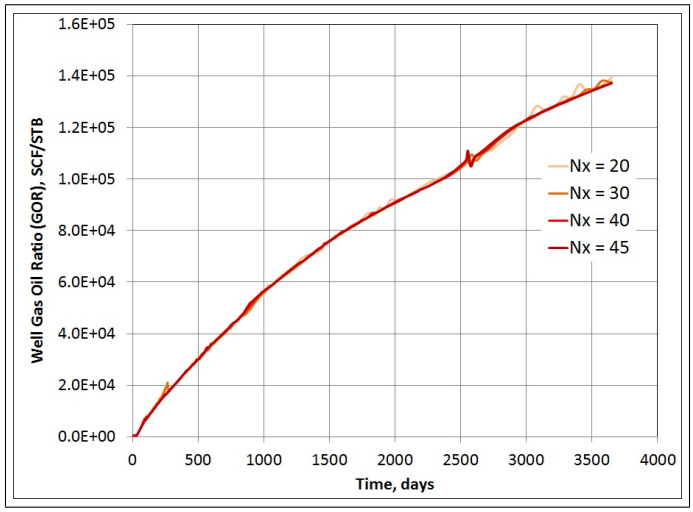

Figure 2.3: GOR Comparison for N_x Sensitivity.

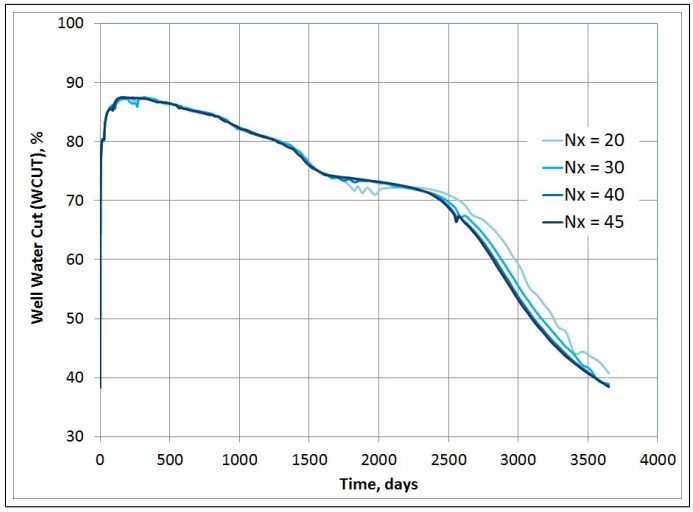

Figure 2.4: Water Cut Comparison for N_x Sensitivity.

Fig. 2.3 and **Fig. 2.4** show the comparison of GOR and water cut with increasing N_x values. As the number of grid in x-direction increase the results start to converge. GOR and water cut from $N_x = 40$ and $N_x = 45$ is in close agreement,

thus it could be conclude that with $N_x = 40$ we already have a converge solution. For future work in this study, $N_x = 40$ will be used in the model.

2.3.2 NZTOP and NZBOTTOM Sensitivity

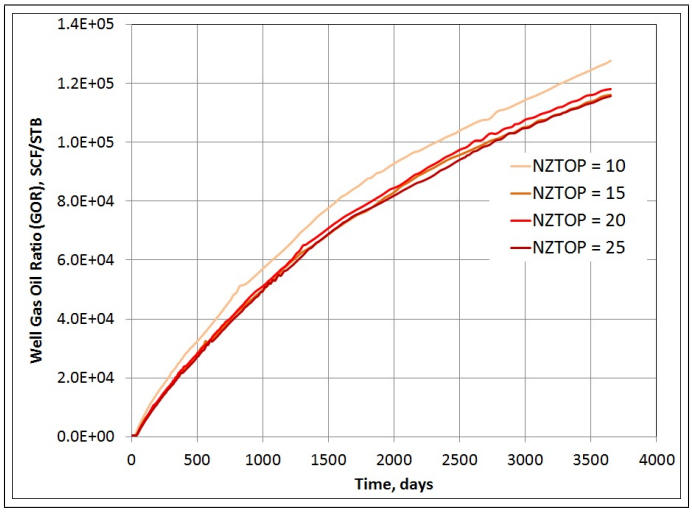

Figure 2.5: GOR Comparison for NZTOP Sensitivity.

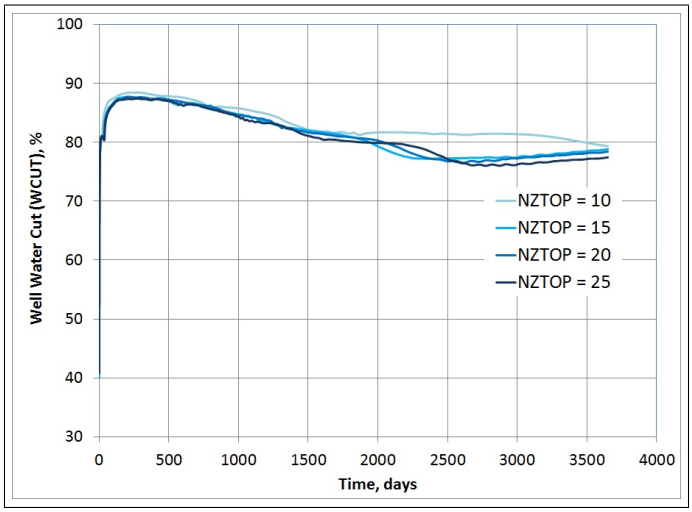

Figure 2.6: Water Cut Comparison for NZTOP Sensitivity.

Since the horizontal well is not mid-centered in z-direction, the sensitivity for the number of grid in z-direction (N_z) was divided into two parts; sensitivity for number of grid from top of reservoir to the well (NZTOP) and from well to the bottom of reservoir (NZBOTTOM). It is important to maintain the fluid contacts to be constant during N_z sensitivity, this to ensure a consistent model (gas, oil, and water initial volumes) when we changing the number of grids. Initial fluid in place from simulator output file could be used for cross–checking.

For NZTOP sensitivity, we used $N_y = 1$, NZBOTTOM = 11, and $N_x = 40$ while NZTOP values is vary from 10 to 25. N_x equal to 40 is taken from previous sensitivity study. GOR and water cut comparison could be seen in **Fig. 2.5** and **Fig. 2.6**. The results start to converge when NZTOP values go from 15 to 25. As the number of NZTOP increase, a converged solution is achieved. Based on this sensitivity study, NZTOP value of 25 could be used in the model to produce a converged solution.

The next step is to conduct NZBOTTOM sensitivity, the value of N_y, N_x, and NZTOP was set to 1, 40, and 25, respectively. While the value of NZBOTTOM is vary from 5 until 14. **Fig. 2.7** and **Fig. 2.8** show the GOR and water cut comparison for NZBOTTOM sensitivity. The solutions start to converge when NZBOTTOM value goes from 11 to 14. It was decided that value of NZBOTTOM = 11 will be used in the base case model since a converged solution could be achieved by using this value.

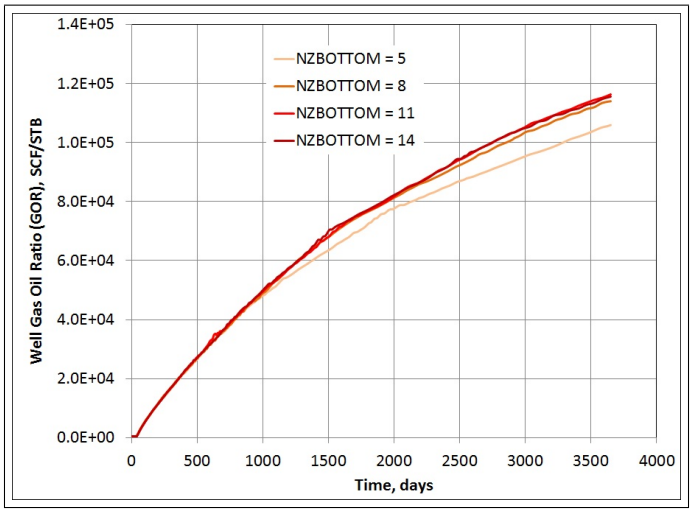

Figure 2.7: GOR Comparison for NZBOTTOM Sensitivity.

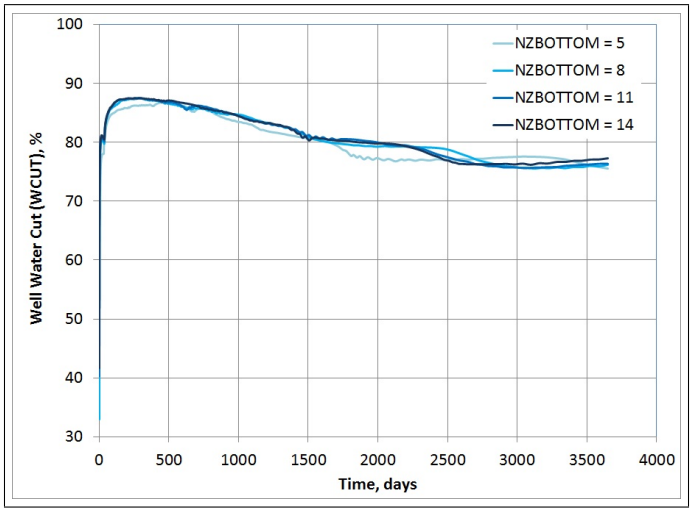

Figure 2.8: Water Cut Comparison for NZBOTTOM Sensitivity.

Based on this grid sensitivity study, for $N_y = 1$, the combination of $N_x = 40$, NZTOP = 25, and NZBOTTOM = 11 could be the optimum grid number to be used. These values are proved to be the number of grid where converge solution is achieved. With this combination of grid number, a total of 1480 grids are used in the model. It should be noted that by using $N_y = 1$, the model will be treated as a 2D problems.

2.4 Implicit Solver Testing

Reservoir model in this study was run in fully implicit mode. This mode will give stable results but require more CPU time, compare to explicit or adaptive implicit modes. The current model, with total of 1480 grid number, has CPU time around 13 seconds. Even though the run time considerably fast, an implicit solver testing still need to be done to observe how the models CPU time vary with different solver options. A shorter CPU time is always preferable since great numbers of simulation run will need to be done. In several cases, tuning is done to make reservoir simulation run faster by changing the numerical parameters. Each simulator has defaults for its numerical parameters that should provide a robust and efficient solution to most simulation problems. To override the defaults with the aim of tuning is not recommended without a good understanding of the solution method involved since it may results in the use of more CPU time.

Table 2.2: Implicit Solver Testing Summary. ILU-011 is the default.

Datafile	Time Steps	Time Steps CUTS	Newton Iterations	Solver Iteration	CPU (sec.)	GOR at 3650 days (SCF/STB)
ILU-000	289	8	662	36341	70.9	124862
ILU-100	247	2	336	10475	19.5	120182
ILU-010	283	9	640	35473	72.8	121003
ILU-001	246	2	341	8534	10.8	120267
ILU-011	**242**	**2**	**339**	**7557**	**8.4**	**120158**
ILU-311	240	2	327	3147	9.9	120034
NF	323	105	680	16303	24.7	120632
D4	255	2	331	0	16.0	120093

There are 3 solver options in Sensor simulator; ILU, Nested Factorization (NF), and D4. For ILU option, the keyword set up is **ILU n n1 n2**; where n is the ILU order, n1 = 1 means to use residual constraint while n1 = 0 means not to use, and n2 = 1 means to use red-black ILU while n2 = 0 means not to use. The default solver is blue ILU-011 or RBILU(0). Detail explanation for ILU solver could be found in [30], while detail explanation for NF and D4 could be found in [7] and [26], respectively.

Table 2.2 provides the summary of implicit solver testing. For this particular model, it was observed that the CPU time, CUTS, and number of iterations will decrease as the ILU order increase. As for the use of residual constraint (by comparing ILU-000 and ILU-010), it was shown that the residual constraint do not helps convergence. But it should be noted that these observation could not be used as generalization. For a given model, there will be a combination of ILU option that could give the least CPU time. A run test (solver testing) will be needed to determine the most efficient solver to be used for particular problem. Based on our observation, the default solver [RBILU(0)] in Sensor is the most efficient solver to be used.

GOR and water cut comparison for solver testing is shown in **Fig. 2.9** and **Fig. 2.10**. It was observed that for this particular problem, the usage of D4, ILU-000, and ILU-010 lead to unstable simulation results. Convergence problem might exist when ILU-000 or ILU-010 option was used; this indicated by large number of solver and Newton iterations **Table 2.2**.

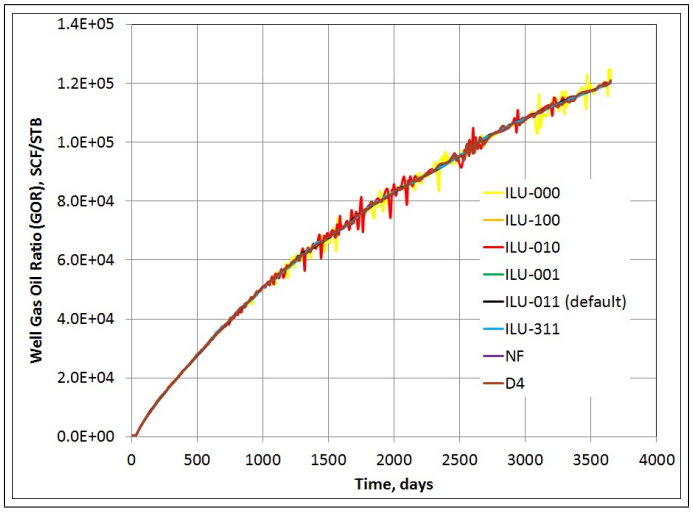

Figure 2.9: GOR Comparison for Implicit Solver Testing.

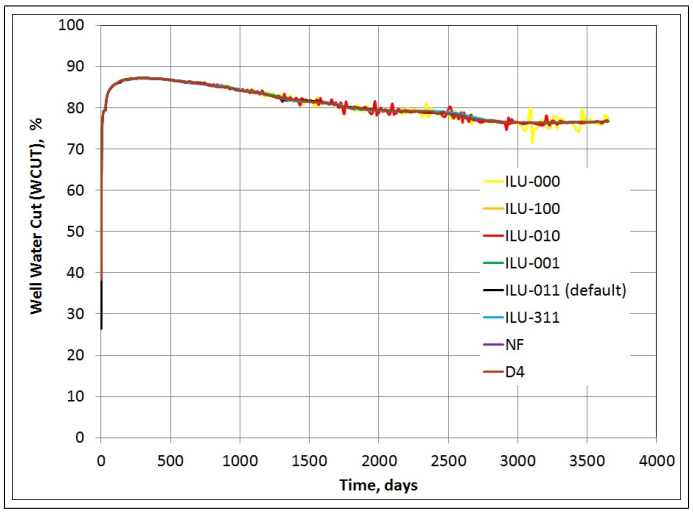

Figure 2.10: Water Cut Comparison for Implicit Solver Testing.

2.5 Base Case Model Description

Base case model will be used to generate the IPR data and also to study the gas and water coning behavior in a thin reservoir underlying big gas cap and overlaying an aquifer. PVT and rock-fluid data used in base case model were taken from reference model (compositional) generated by Dr. Alexander Juell, these data correspond to the Troll field example. A conversion from compositional to black oil was done

Table 2.3: Base Case Model Description.

Depth top gas zone	DTOP	5000 ft
Depth bottom of the reservoir	DBOTTOM	5150 ft
Depth of the well	DWELL	5095 ft
Gas oil contact	GOC	5050 ft
Water oil contact	WOC	5100 ft
Total length in x-direction	L_x	1000 ft
Total length in y-direction	L_y	3280 ft
Total length in z-direction	L_z	150 ft
Number of grids in x-direction	N_x	40
Number of grids in y-direction	N_y	1
Number of grids in z-direction	N_z	37
Horizontal permeability	k_h	1000 mD
Ration of vertical and horizontal permeability	k_v/k_h	0.25
Porosity	ϕ	0.25

for the base case model. The initial pressure in the model was set at bubble point pressure. **Table 2.3** provides several reservoir data that being used in base case model.

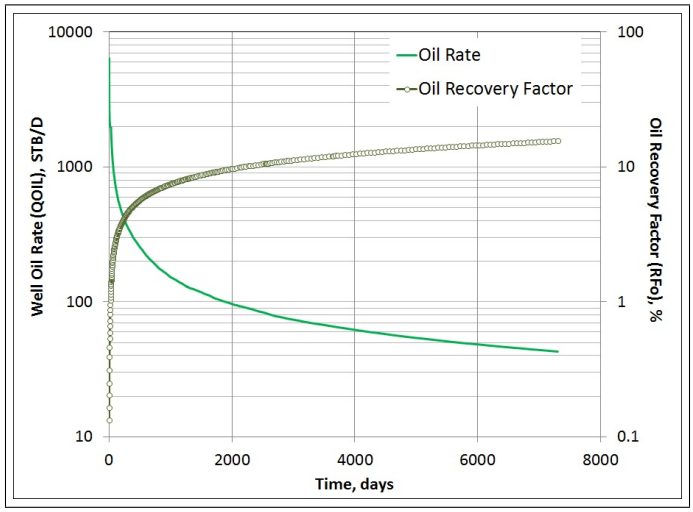

Figure 2.11: Base Case Model: Oil Rate and Oil Recovery Factor versus Time.

Reservoir model has 150 ft total thickness; 50 ft each for gas, oil, and water zone. To simulate big gas cap and aquifer, a very large porosity value was set at the top-most and bottom-most grid layer. Gas cap and aquifer volume can

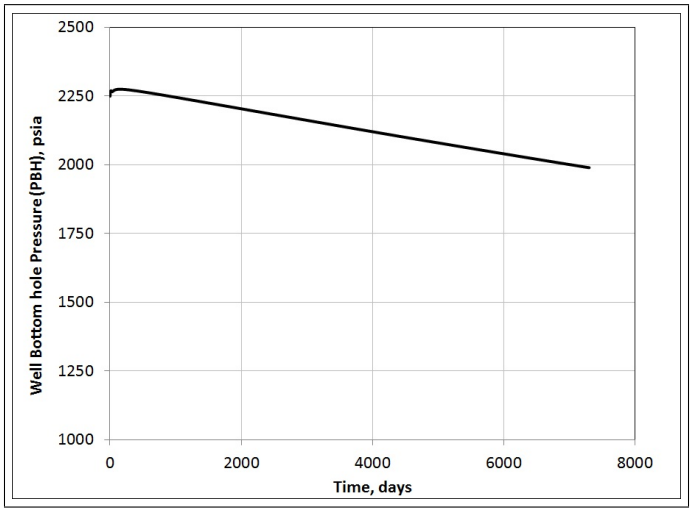

Figure 2.12: Base Case Model: Bottom-hole Pressure versus Time.

be adjusted by changing the thickness of these layers. One horizontal producer well were completed along y-direction, located at grid ($i = 1, j = 1, k = 26$), and perforated 5 ft above WOC. This well produces at minimum BHP of 1500 psia and maximum oil rate of 10000 STB/D.

Fig. 2.11 and **Fig. 2.12** present the oil rate, oil recovery factor, and flowing bottom-hole pressure versus time for base case model. The oil rate decrease rapidly in the first two years; after 20 years of production the oil rate go down to 43 STB/d. Major recoveries was achieved at first 10 years, afterward, the oil recovery increase in a slow rate and achieve 16% after 20 years of production. The reservoir pressure decreases $\pm$300 psia in 20 years.

Gas and water breakthrough occurs in the early period of production. Severe gas coning indicated by a rapid increase of GOR in the production well (**Fig. 2.13**). The water breakthrough indicated by sharp increase of water, after some times the water cut decrease and become relatively stable at 80% (**Fig. 2.14**). When the well starts producing higher than the critical rate; the coning (gas and water) occurs. High pressure from big gas cap pushes the oil down to water zone. In consequences; the GOR increases rapidly and the oil rate decreases. While the water cut, after the breakthrough and sharp increase in water cut occurs, gas coning start to dominate the flow (due to high pressure from gas cap). This might be the reason why the water cut decrease after breakthrough happened.

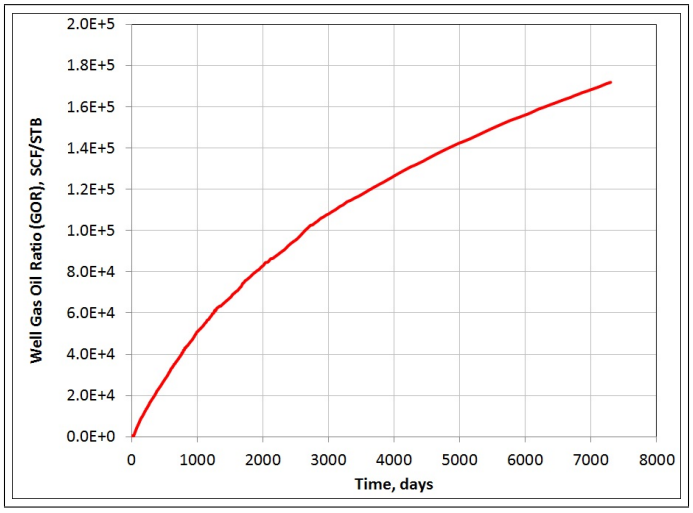

Figure 2.13: Base Case Model: Gas Oil Ratio versus Time.

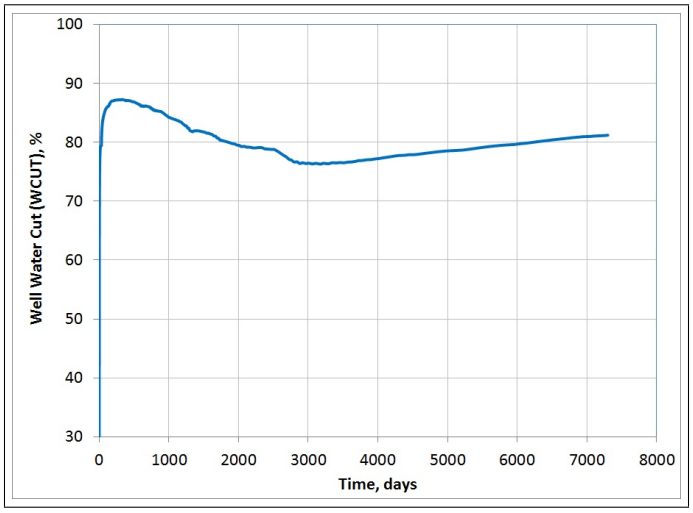

Figure 2.14: Base Case Model: Water Cut versus Time.

Fig. 2.15 shows the saturation snapshot for base case model producing at 0 day (A), 1 year (B), 10 years (C), and 20 years (D). Using this snapshot, we could observe how the coning evolve and behave with time. Interesting observation that we found is that as depletion proceeds, the gas from the gas cap expand and push the oil column to the water zone.

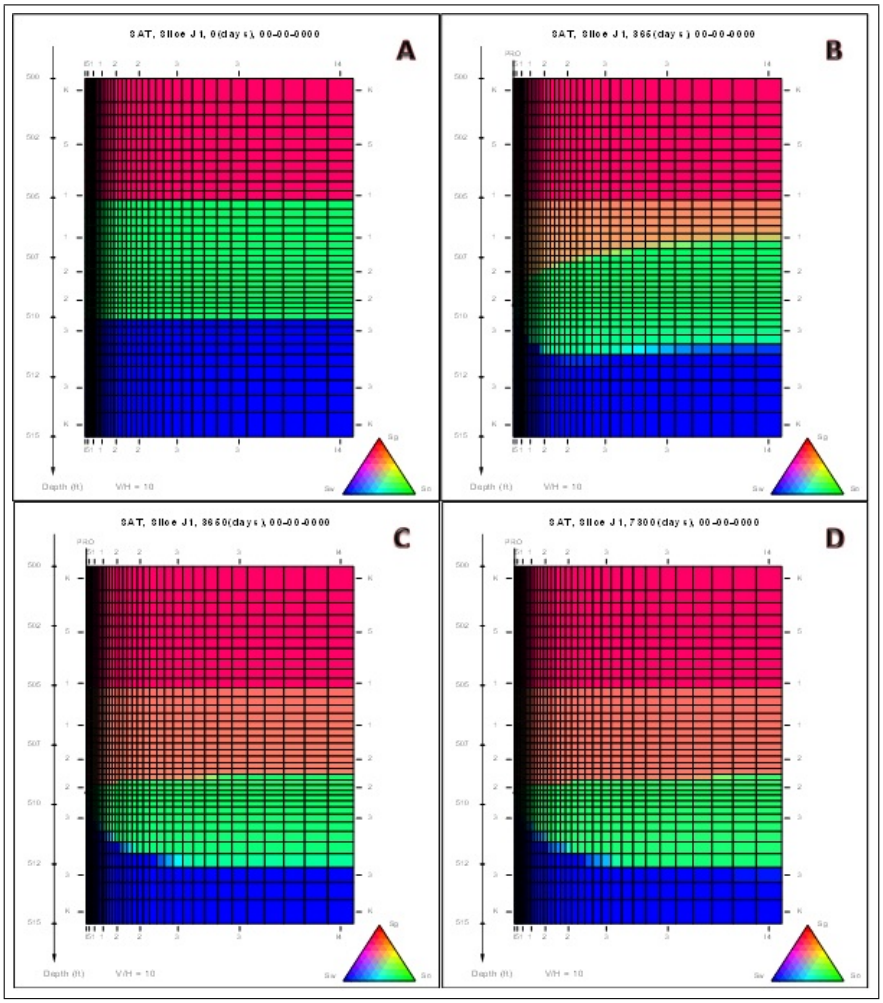

Figure 2.15: Saturation Snapshot of Base Case Model (IK-cross section).

Chapter 3

WATER AND GAS CONING IN HORIZONTAL WELL

3.1 Introduction

Several analytical studies indicate that horizontal well usually have higher productivity than vertical well, this mainly due to longer length open to flow [8, 11, 24]. In a thin oil reservoir, horizontal wells were proposed as an alternative to vertical wells. Coning occurs when a pressure gradient near the perforated interval exceeds the gravity head from fluid density differences. The long length, increased areal sweep and increased productivity of the horizontal well could reduce this pressure gradient; thus reducing the coning problems and improve the oil recovery.

In reservoir with thin oil column, sandwiched between big gas cap and aquifer, gas and water coning most likely will occurs during oil production. Since the critical rates usually very low (and un-economic), the well usually produce at rate higher than the critical rates. This makes coning problems un-avoidable. In this project, several sensitivity studies were done to better understand the coning behavior for horizontal well produce from thin oil reservoir underlying big gas cap and overlaying an aquifer.

In general, coning behavior depends on thickness of oil column, density contrast between oil and coning fluids, oil viscosity, effective permeability, and the size of gas cap and/or aquifer strength. In this chapter, only last three parameters will be discussed in detail based on sensitivity results.

3.2 Permeability Sensitivity

Permeability sensitivity divided into 2 sections, horizontal permeability sensitivity and ratio of vertical to horizontal permeability sensitivity. The base case model will be used with only one parameter is changed per simulation run. The objective is to observe the effect of permeability on water and gas coning in thin oil reservoir sandwiched between gas cap and aquifer.

3.2.1 Horizontal Permeability Sensitivity

Four cases were run with different horizontal permeability values (250 mD, 500 mD, 1000 mD, and 2000 mD) and constant k_v/k_h value of 0.25. Other parameters in base case model are remains constant. **Fig. 3.1** and **Fig. 3.2** show that higher horizontal permeability will results in higher oil rate, thus higher oil recovery.

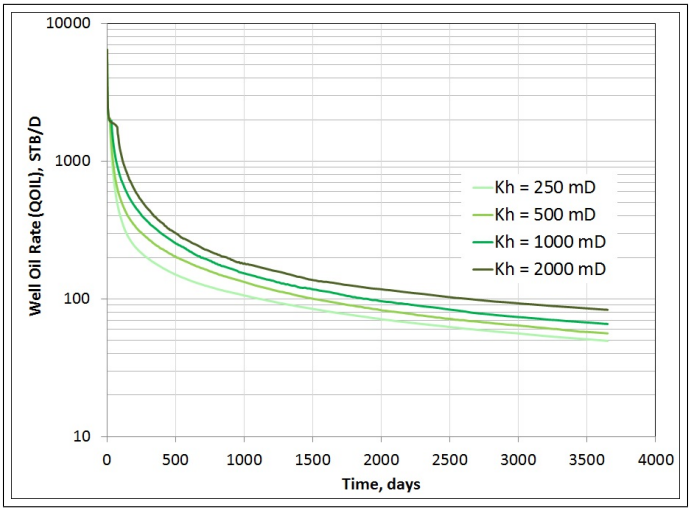

Figure 3.1: Horizontal Permeability Effect on Oil Rate.

From **Fig. 3.3** and **Fig. 3.4**, we could see that increase in horizontal permeability will delays gas and water coning. It also observed that the higher the

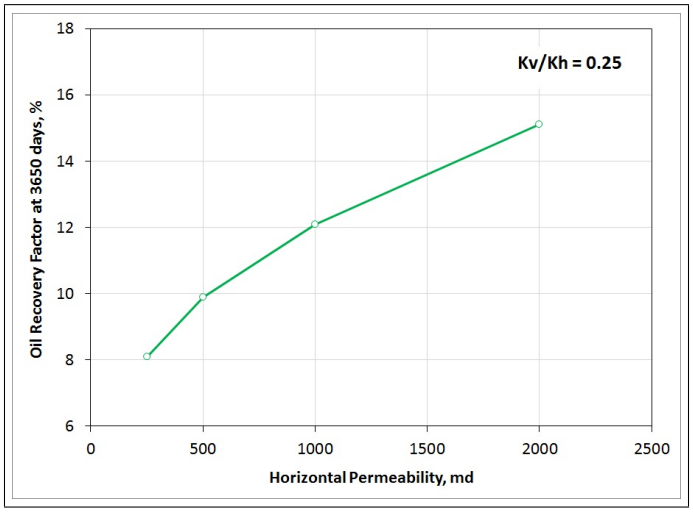

Figure 3.2: Oil Recovery Factor at 10 years versus Horizontal Permeability.

horizontal permeability, the lower the GOR and/or water cut after breakthrough. In a reservoir with high horizontal permeability, the fluids will tend to flow in horizontal direction than vertical direction. This will reduce the tendency of gas and water to cone into the well. In consequences, the breakthrough time and critical rate will be higher and the coning-fluid production after breakthrough will be lower.

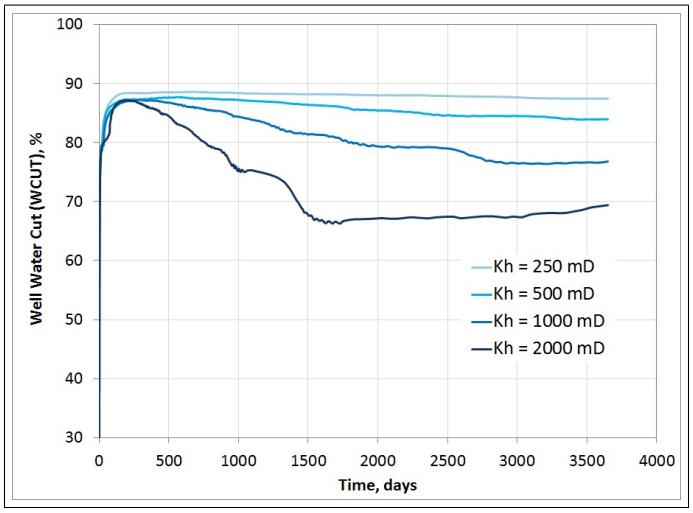

Figure 3.3: Horizontal Permeability Effect on Water Cut.

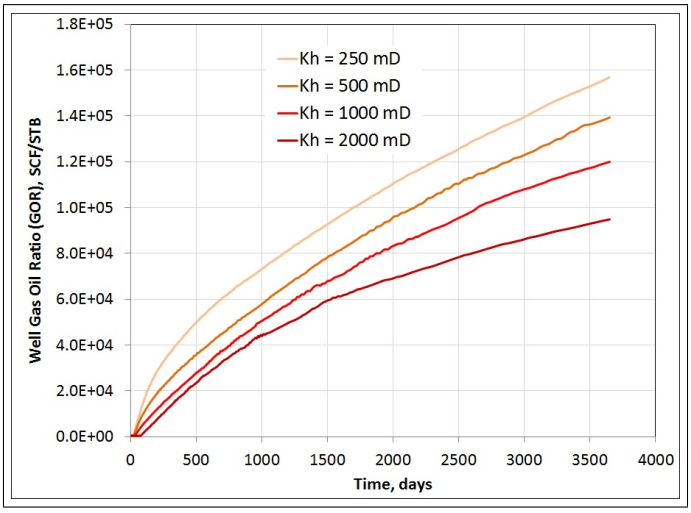

Figure 3.4: Horizontal Permeability Effect on GOR.

In summary, the higher the horizontal permeability, the higher the cumulative production, the longer the breakthrough time, and the lower the gas and water production. The tendency of gas and water coning in high horizontal permeability reservoir is less than in low permeability reservoir.

3.2.2 k_v/k_h Sensitivity

In k_v/k_h sensitivity, the base case model was run with five different k_v/k_h values. These values vary from 0.1 to 1.25. The case with $k_v/k_h = 1.25$ was included to study the coning behavior when vertical permeability is higher than horizontal permeability. The first sensitivity will be done with $k_h = 1000$ mD, and the second with $k_h = 300$ mD.

From **Fig. 3.5**, we could conclude that in reservoir with high horizontal permeability ($k_h = 1000$ mD), there is only slight effect of vertical anisotropy ratio on gas breakthrough time and the GOR after breakthrough. The high mobility of gas might cause this behavior. In this case where $k_h = 1000$ mD, even small vertical anisotropy ratio results in vertical permeability of 100 mD. With its high mobility, this much of vertical permeability will allow gas to flow/cone into the well, as easy as when the vertical permeability is higher.

Fig. 3.6 show that in reservoir with high k_h, the vertical anisotropy ratio affect the water cut after breakthrough. Increase of k_v/k_h value will result in higher water cut when breakthrough happen but then the water cut will decrease

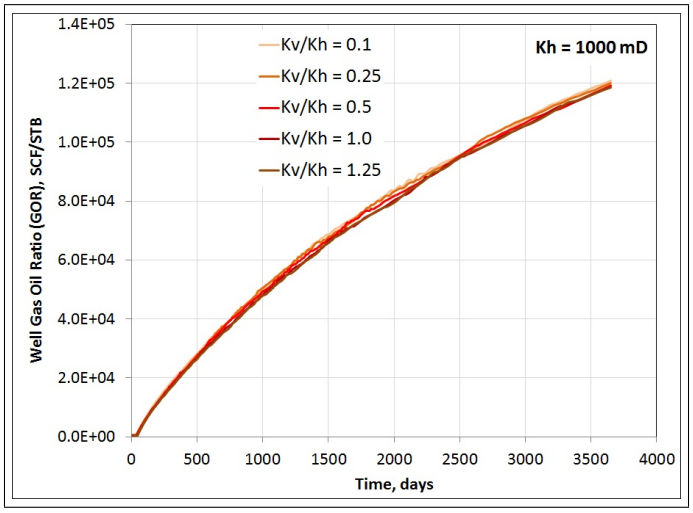

Figure 3.5: k_v/k_h Effect on GOR for $k_h = 1000$ mD.

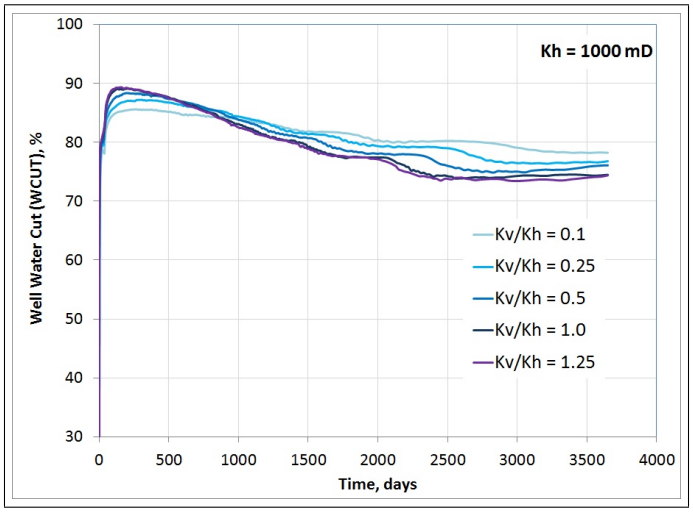

Figure 3.6: k_v/k_h Effect on Water Cut for $k_h = 1000$ mD.

(faster) when k_v/k_h increase. It might relate with the fact that after some times, gas from gas cap pushes oil to the water zone causing the WOC to shift further away from perforation point.

Fig. 3.7 and **Fig. 3.8** show the GOR and water cut profiles for k_v/k_h sensitivity in reservoir with $k_h = 300$ mD. From GOR profile, we could see that higher vertical anisotropy ratio will results in early gas breakthrough but slower increase of

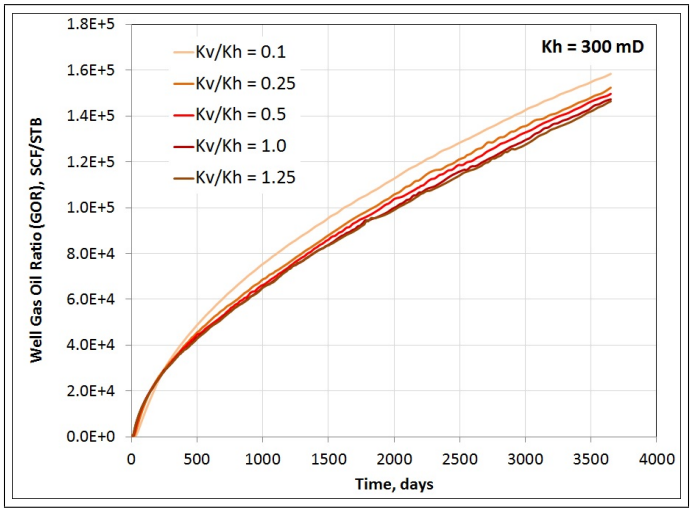

Figure 3.7: k_v/k_h Effect on GOR for $k_h = 300$ mD.

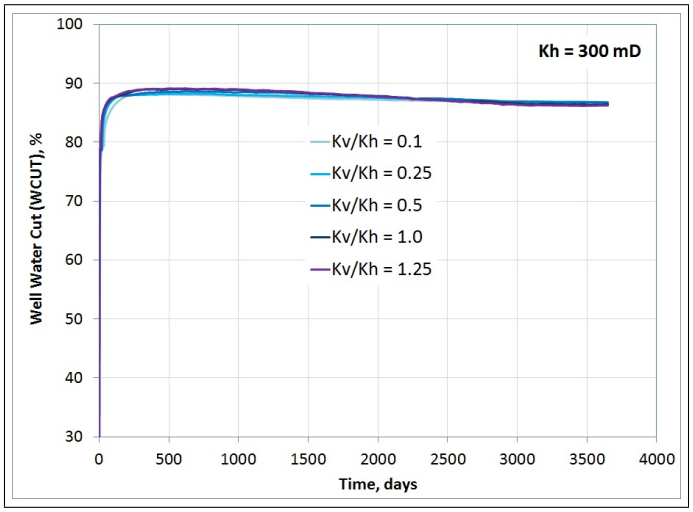

Figure 3.8: k_v/k_h Effect on Water Cut for $k_h = 300$ mD.

GOR. From water cut profile, it was found that there is only slight effect of vertical anisotropy ratio on water breakthrough time and water cut after breakthrough.

From plot of oil recovery factor versus k_v/k_h (**Fig. 3.9**), we could conclude that for k_v/k_h lower than 0.2, the decrease of k_v/k_h results in lower oil recover factor. But for k_v/k_h higher than 0.2, it appears that the vertical anisotropy ratio value only has slight effect on oil recovery factor. There is only 0.1 – 0.3% difference on

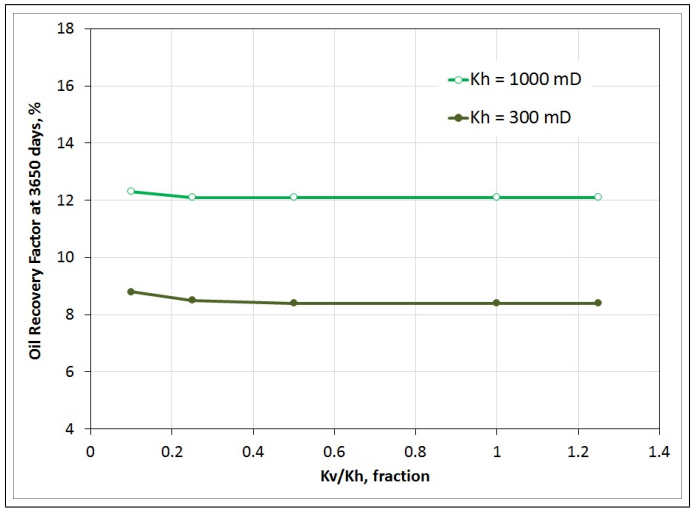

Figure 3.9: Oil Recovery at 3650 days versus k_v/k_h for Different k_h Values.

oil recovery for k_v/k_h values of 0.1 to 1.25. These conclusion apply for reservoir with $k_h = 1000$ mD and $k_h = 300$ mD.

3.3 Gas Cap and Aquifer Size Sensitivity

To better understand the coning behavior in thin oil reservoir underlying a gas cap and overlaying an aquifer, a sensitivity of gas cap and aquifer size was done. The size of gas cap and aquifer are represented by the initial volume of gas and water. In Sensor data file, the size of gas cap and aquifer was changed by modifying the gas cap and aquifer height.

Gas cap size sensitivity will be discussed first in this section. The sensitivity was done by using the base case model and run it using Sensor with different gas cap height value per simulation run. Results from this sensitivity study are presented below.

Fig. 3.10 shows that the size of gas cap only has slight effect the oil rate. Increase in gas cap size will results in lower oil rate. The existence of gas cap usually help in reservoir pressure support/pressure maintenance. As we can see from **Fig. 3.11**, bigger gas cap size will provide more pressure support in reservoir. Reservoir pressure decrease faster when the gas cap size is smaller.

Fig. 3.12 and **Fig. 3.13** show that the gas cap size does not affect the water and gas breakthrough time. Different gas cap sizes give approximately the same

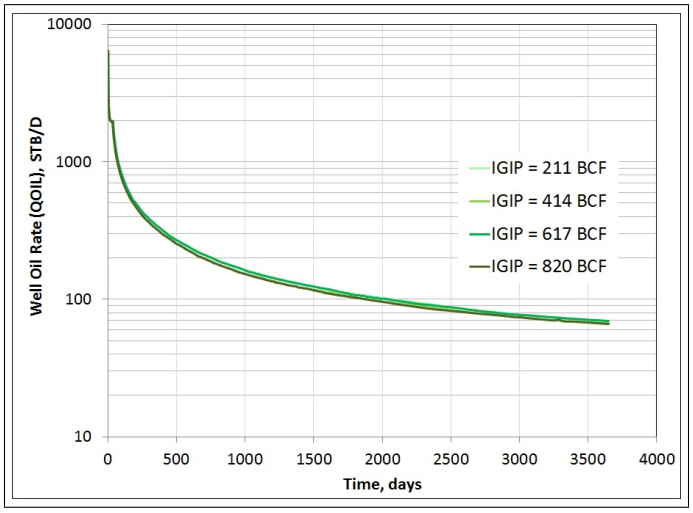

Figure 3.10: Gas Cap Size Effect on Oil Rate.

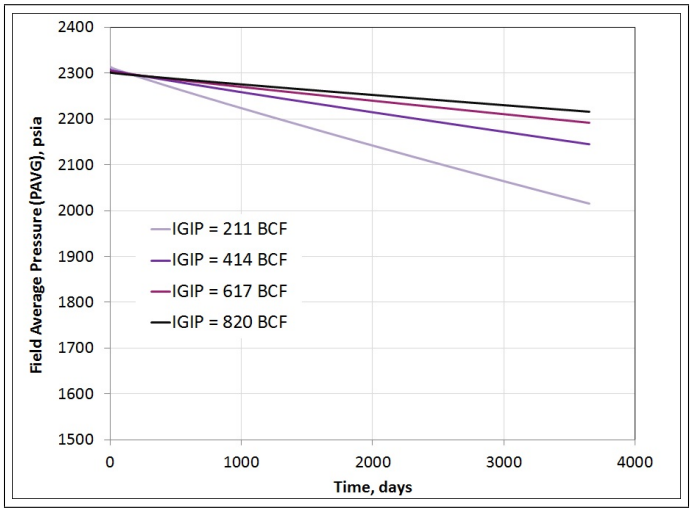

Figure 3.11: Gas Cap Size Effect on Field Average Pressure.

breakthrough time. Whereas, the trends of GOR and water cut after breakthrough is affected by gas cap size. Bigger gas cap size results in higher GOR but lower water cut.

When bigger gas cap exist in reservoir, gas production due to coning will be higher. Excessive gas production could dominate the flow in well, in consequences, the oil and water production will decrease. There is also a possibility where a

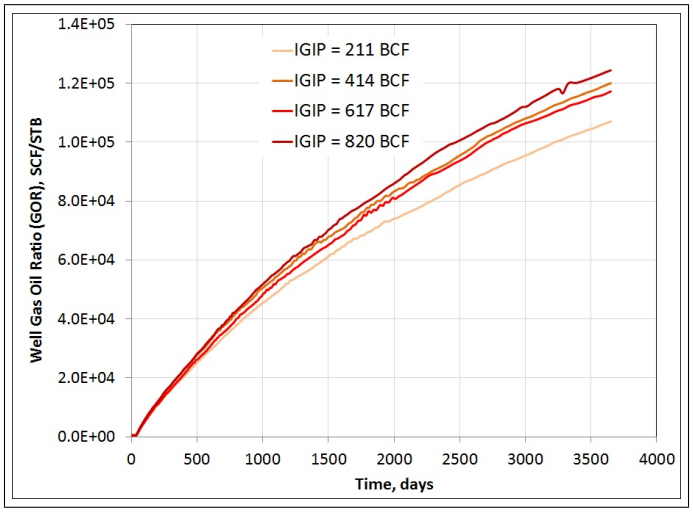

Figure 3.12: Gas Cap Size Effect on GOR.

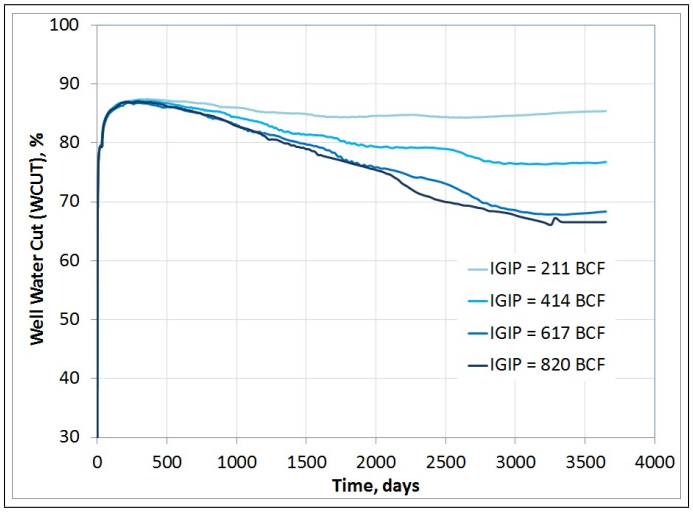

Figure 3.13: Gas Cap Size Effect on Water Cut.

bigger gas cap could push oil further down into the water zone. When this happen, the distance between perforation point and WOC will be longer thus resulting in lower water production or lower water cut.

Increase in gas cap size will results in lower oil recovery factor (**Fig. 3.14**). Even though bigger gas cap can give more pressure support in reservoir, it can also cause more gas production from coning. When the gas dominates flow into the well,

the oil production will decrease. In consequences the cumulative oil production (oil recovery) is lower.

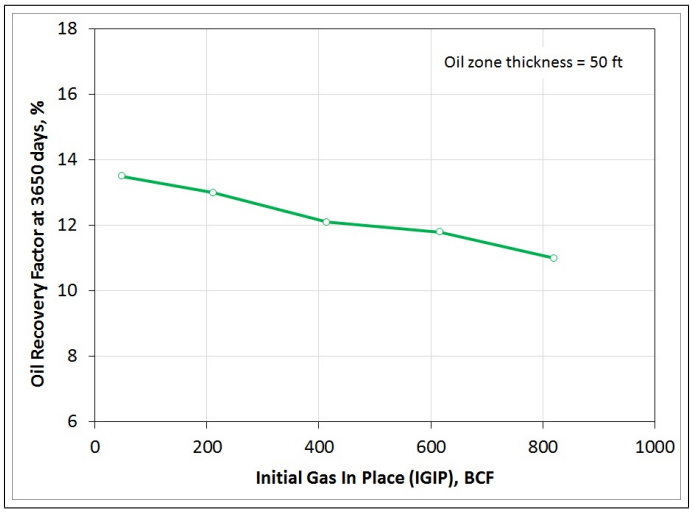

Figure 3.14: Oil Recovery at 3650 days versus Initial Gas In Place (IGIP).

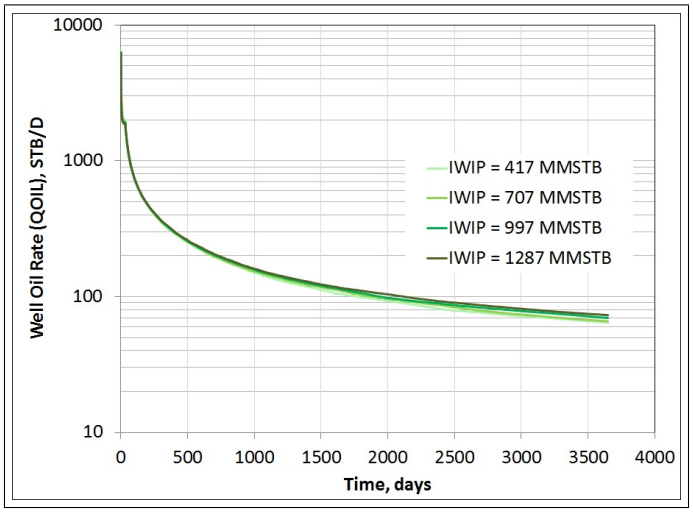

Figure 3.15: Aquifer Size Effect on Oil Rate.

Aquifer size sensitivity will be discussed in this section. The sensitivity was done by using the base case model and run it using Sensor with different aquifer size per simulation run. The aquifer size was changed by modifying the bottom-most grid block height.

Fig. 3.15 show that aquifer size has slightly effects on oil rate, especially at the later stage of production. Bigger aquifer size will results in higher oil rate, thus higher cumulative oil production. There is also slight effect of aquifer size to reservoir pressure. Higher oil rate more likely caused by aquifer size effect on coning behavior than due to pressure maintenance by aquifer.

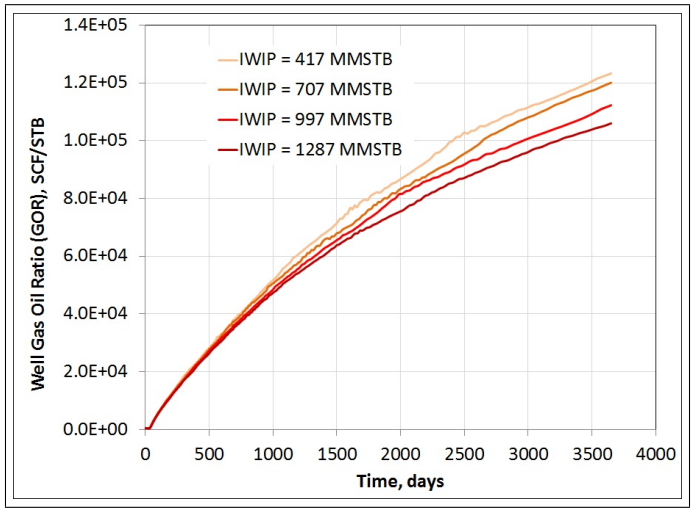

Figure 3.16: Aquifer Size Effect on GOR.

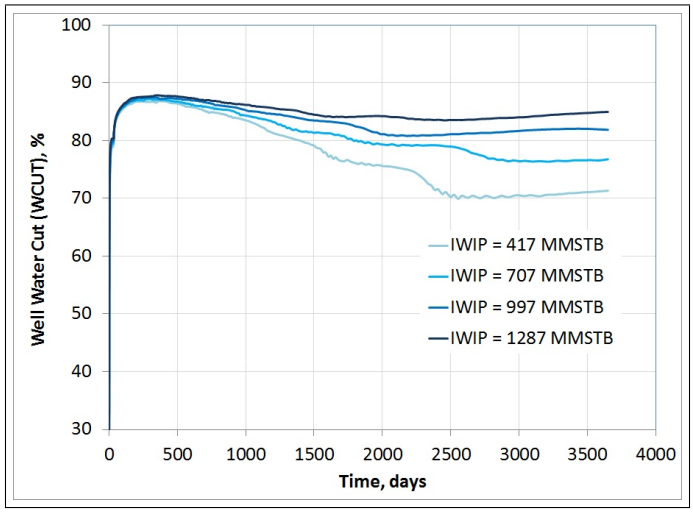

Figure 3.17: Aquifer Size Effect on Water Cut.

Fig. 3.16 and **Fig. 3.17** show that aquifer size affect the GOR and water cut after breakthrough. But it was observed that aquifer size does not affect the gas and water breakthrough time. Different size of aquifer will give approximately the same breakthrough time. Increase in aquifer size will leads to higher water cut. This is because the tendency of water coning is increase when we have bigger aquifer. For constant gas cap size, bigger aquifer will results in lower GOR.

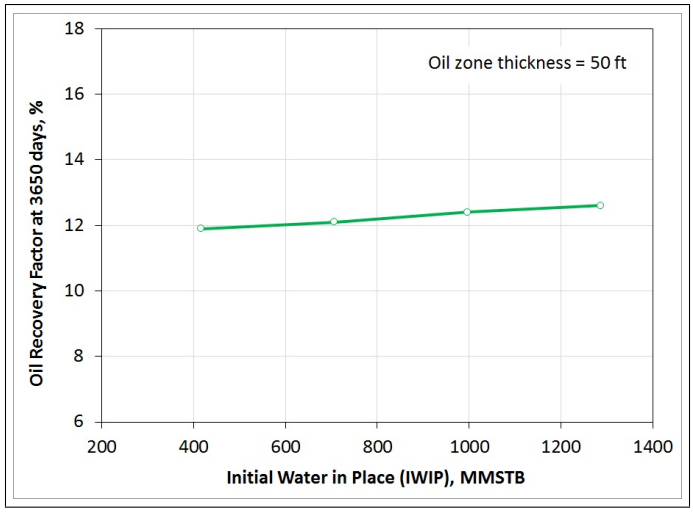

Figure 3.18: Oil Recovery Factor at 3650 days versus Initial Water In Place (IWIP).

Fig. 3.18 shows the effect of aquifer size on oil recovery factor. We can see that there is only slight effect of aquifer size on oil recovery. With tripled aquifer volume, the oil recovery increase less than 1%. The aquifer size affect mostly on gas and water coning behavior. Bigger aquifer size will increase the tendency of water coning and reduce the tendency of gas coning. Excessive water production should be expected if we have big aquifer, especially when the horizontal well is completed closer to WOC.

3.4 Well Placement Optimizations

To minimize coning problem, horizontal well usually drilled away from the fluid contact. In a case where the oil column sandwiched between gas cap and aquifer, well optimization study will need to be done to determine the optimum well placement. This could be done by utilizing numerical simulator or by using an analytical method. Papatzacos et. al. [25], proposed an analytical method to calculate the

optimum well placement, where the gas and water coning will breakthrough at same time. But practically, delaying a gas breakthrough is the main concern. Over time, gas breakthrough can dominate flow in the well and cause reduction in oil rate. Excessive gas production from gas cap can also cause rapid pressure decline in reservoir. **Fig. 3.19** shows the horizontal well placement in our base case model. The well was located 5 ft away from WOC and 45 ft away from GOC.

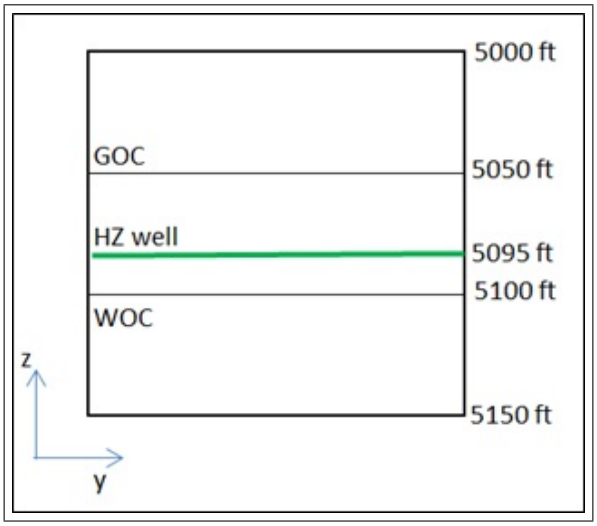

Figure 3.19: Well Placement in Base Case Model.

Base case model was run with different well depth using Sensor. The oil recovery factor for each well depth at 1, 5, 10, 20, and 30 years was recorded and plotted on XY-chart **Fig. 3.20**. An interesting observation from this figure is that the trends of oil recovery factor changes with time. If we only consider one year production, the optimum well placement is in the lower one-third section of the oil leg. In field application, usually this is where the horizontal well is drilled. But the oil recovery trends are changes with time; in a long production period, it appears to be beneficial to place horizontal well in upper section of the oil leg. If we consider 20 years of production, the optimum well placement will be around upper two-fifth section of the oil leg.

These observations should not be made as generalization since it was generated only using one set data of reservoir model. There might be different trends of oil recovery factor for different reservoir and horizontal well configuration. We recommend generating the plot based on your particular reservoir, development plan, and well configuration data; and use it as a tool to help in deciding the optimum well

placement. Several factors that might effect on optimum well placement are oil flow rate, oil viscosity; oil FVF, density difference between reservoir fluid, perforation interval lengths, mobility ratio, and the gas cap and aquifer size [32].

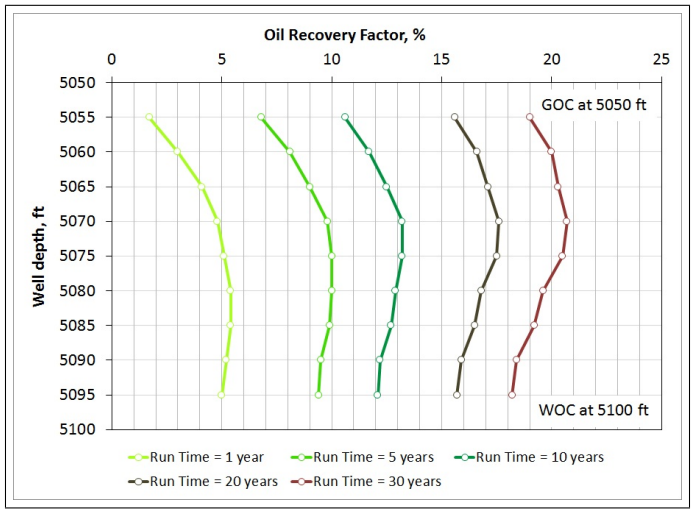

Figure 3.20: Oil Recovery versus Well Depth at Different Run Time.

The production profiles of horizontal well (**Fig. 3.21** – **Fig. 3.23**) could help to explain the trends that we saw on oil recovery plot versus well depth. When the well is placed closer to WOC, the water production will increase significantly at early time. The gas coning will be delayed but after the breakthrough happen, the gas production will increase rapidly with time. These results in decreasing oil rate. And when the well is placed closer to GOC, the gas breakthrough will happen at early time and the gas production will increase with time, but less rapid than the gas production from the well closer to WOC. The water breakthrough will be delayed, but after the breakthrough happen water production will increase. Water cut is higher for the well closer to WOC. The oil rate will decrease with time when the coning occurs. But since there are less gas and water coning, the oil rate is higher than the well completed closer to WOC. This will result in higher cumulative oil production and oil recovery.

Another alternative for optimal horizontal well placement in thin oil reservoir sandwiched between big gas cap and aquifer is to drill the well below WOC. This method proposed by Haug, B. T. et. al. [16] based on simulation study for Troll Well Gas Province. Well placement below WOC relies on what they called inverse coning process, this is when there is a down-coning of oil into the well through the

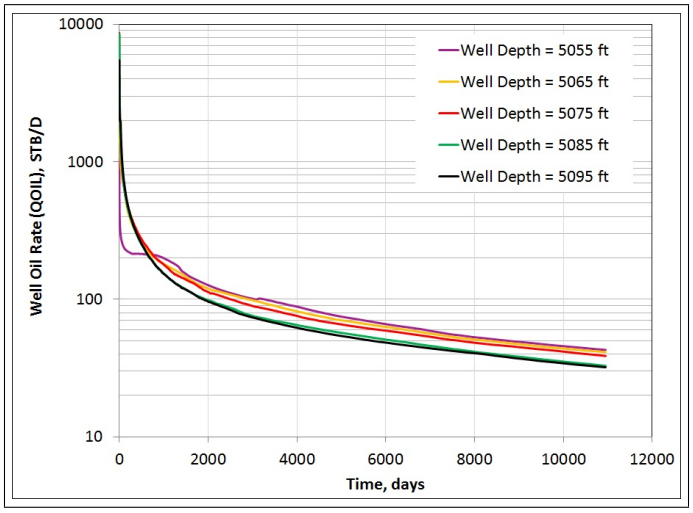

Figure 3.21: Oil Rate Profile for Different Well Depth.

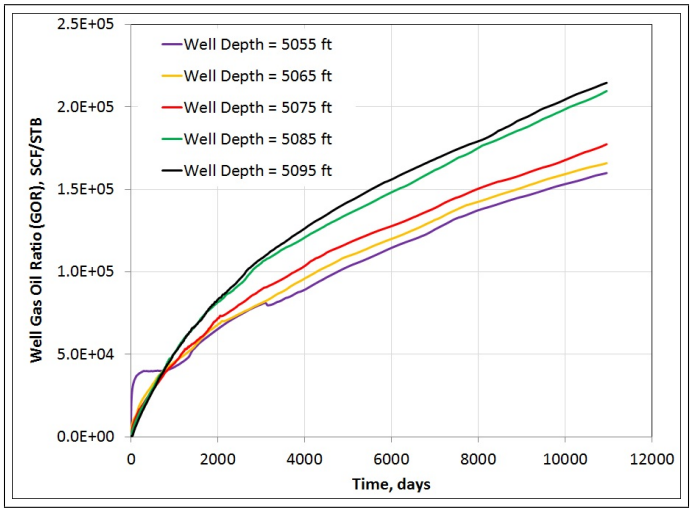

Figure 3.22: GOR Profile for Different Well Depth.

water zone. This method will also expect to delay the gas breakthrough. Unfortunately no saturation maps that showing this inverse coning process presented in the paper.

The well placement below WOC was also studied using the base case model. For this exercise, we place the well 10 ft below WOC and let it produce for 20 years. To observe the coning behavior, saturation map in IK-section was generated

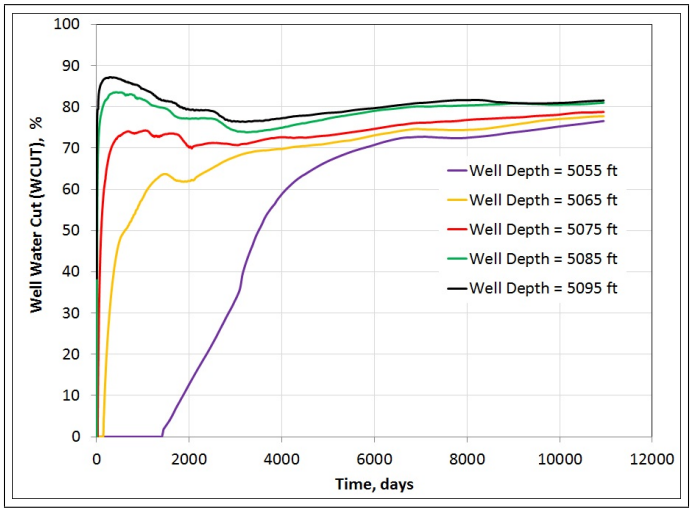

Figure 3.23: Water Cut Profile for Different Well Depth.

for different run time (**Fig. 3.24**). From saturation map at 40 days, we could see that 'inverse coning' does happen when we place the well below WOC. But we also observed that the gas from gas cap pushes oil into the water zone. Along with time, the oil column is shifted to the perforation point (saturation map at 365 days). When this happen, the production actually comes from well that produce from oil zone with gas and water coning, instead from well produce from water zone with 'inverse coning' of oil and gas.

To summarize, when we place the horizontal well below WOC, 'inverse coning' of oil to the well will happen in early period. But when the gas pushes the oil to the water zone, the well actually produces from an oil zone with gas and water coning. So the inverse coning contributes in oil recovery at early period, but the oil recovery at later stage relies on gas from gas cap that pushes the oil to water zone. The combination of these mechanisms gives the oil recovery factor around 14% after 20 years of production. This is lower than the recovery of the well completed at upper section of the oil leg. And enormous water production should be expected when the well is completed below WOC.

3.5 Coning Collapse Study

In a thin oil reservoir underlying a gas cap and overlaying an aquifer, gas and water coning could be un-avoidable problems. Especially in many cases, the well

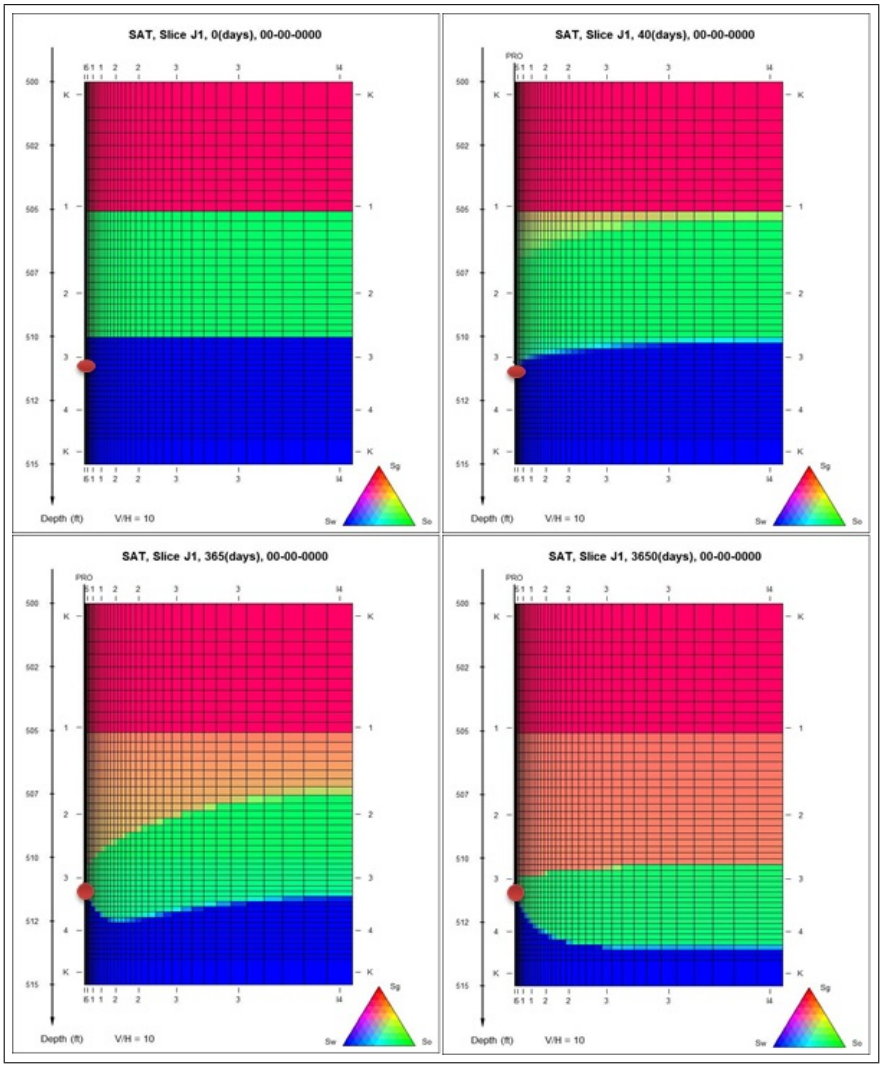

Figure 3.24: Saturation Map at Different Run Time for Horizontal Well Completed Below WOC.

is produced above critical rate. It is usually uneconomical to keep well production rate below the critical rate.

When gas and water production from coning start dominate the production stream, the oil production will decrease. At some point, high GOR and/or water cut becomes uneconomical and a well may need to be shut-in to allow the cone return to a sharp interface. This condition at which the cone return to sharp

interface and the fluid interface subsided is called cone subsidence or cone recession. In this study, we use term coning collapse. The optimum shut-in time depends on the subsidence time of the water/gas cone.

Lee and Permadi [22] proposed an analytical solution to determine the water cone subsidence time. They solved the diffusivity equation using the separation of variables technique to determine the instantaneous cone height after the well is shut. Other solutions to determine cone receding time was proposed by Ibelegbu et. al. [18].

Shutting the well will results in revenues losses, especially if the production stopped for long period. In field application, chocking the well to lower flowing bottom-hole pressure has become one alternative to reduce coning problems. By lowering flowing bottom-hole pressure, the wellbore drawdowns will decrease. In consequence, the dynamic force that causes coning will be reduced.

In this study, we use numerical simulation and the base case model to find the flowing bottom-hole pressure value for certain reservoir pressure when the cone collapses ($P_{wf_{cc}}$). To find the $P_{wf_{cc}}$ value, we could increase the bottom hole pressure (BHP) value at certain time to simulate well chocking, and do trial and error to find BHP value when the cone collapse (water cut or GOR becomes $\sim$ zero). But this method is not effective since it will need numerous trial and errors.

We decided to use different approach, we set a constant bottom-hole pressure on well model and let it run until the water cut or GOR becomes zero (or a very small value). We define the bottom-hole pressure constraint on well model as $P_{wf_{cc}}$. The reservoir pressure when the water cut decrease to zero (when water cone collapse) was then recorded. This reservoir pressure is defined as $P_{R_{cc}}$ for water coning. The reservoir pressure when the GOR decrease to zero (when gas cone collapse) was also recorded. This reservoir pressure is defined as $P_{R_{cc}}$ for gas coning.

The ratio of $P_{wf_{cc}}$ to $P_{R_{cc}}$ was then calculated and defined as $\left(\frac{P_{wf}}{P_R}\right)_{cc}$, the ratio of bottom-hole pressure to reservoir pressure at which the cone start to collapse. For practical purposes, a curve that correlates $\left(\frac{P_{wf}}{P_R}\right)_{cc}$ with reservoir pressure was generated, each for gas coning and water coning (**Fig. 3.25**).

Fig. 3.25 show that the ratio of bottom-hole pressure to reservoir pressure at which the cone start to collapse, $\left(\frac{P_{wf}}{P_R}\right)_{cc}$ is lower when the reservoir pressure decrease. It is also observed that for particular reservoir pressure, $\left(\frac{P_{wf}}{P_R}\right)_{cc}$ is higher for water coning than gas coning. This means, compare to gas cone collapse, higher bottom-hole pressure will be needed to make the water cone collapse. This observation is agreed with the coning theory. With constant reservoir pressure, higher

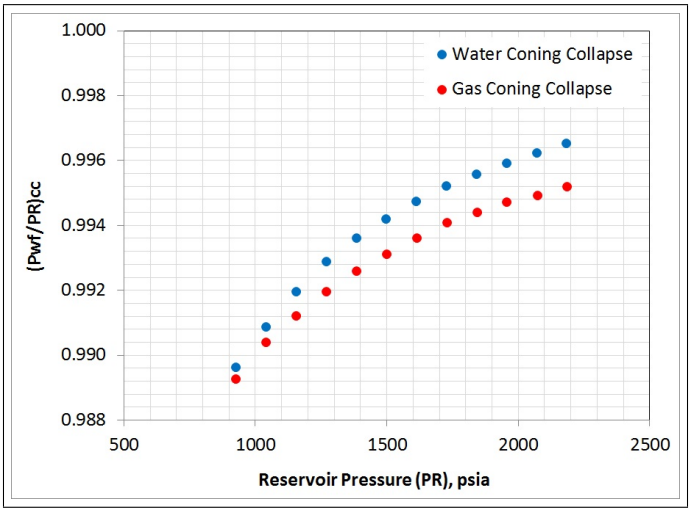

Figure 3.25: Relationship between Reservoir Pressures and Flowing Bottom-hole Pressure When the Cone Collapse.

bottom-hole pressure will results in smaller drawdown in the wellbore. Theoretically, the coning tendencies are inversely proportional to the density difference of the fluids. Since the density different between water and oil is smaller than the density difference between gas and oil, water has more tendency to cone than gas. Thus, smaller drawdown is needed to prevent water to cone.

The value of $\left(\frac{P_{wf}}{P_R}\right)_{cc}$ that close to one means that a very small drawdown will be needed to allow the cone to collapse. A very small drawdown will results in a very low production rate. This low production rate might represent the critical rate for the gas and water coning. *Critical rate is the rate above which the flowing pressure gradient at well causes water (or gas) cone into the well* [6].

3.6 Coning Effect on Maximum Producing Rate

Gas and water coning could be serious problem in and oil field. Coning can reduce the well productivity significantly and has negative impact on recovery efficiency of the oil reservoir. The depletion mechanism is also reduced when coning happen, this lead to loss of total field recovery. We present the study on how the coning affects the well maximum producing rate; each for oil, water, and gas phase. The study on how the coning affect the maximum production rate was done by comparing the maximum rate between the coning model (base case) and the single phase model.

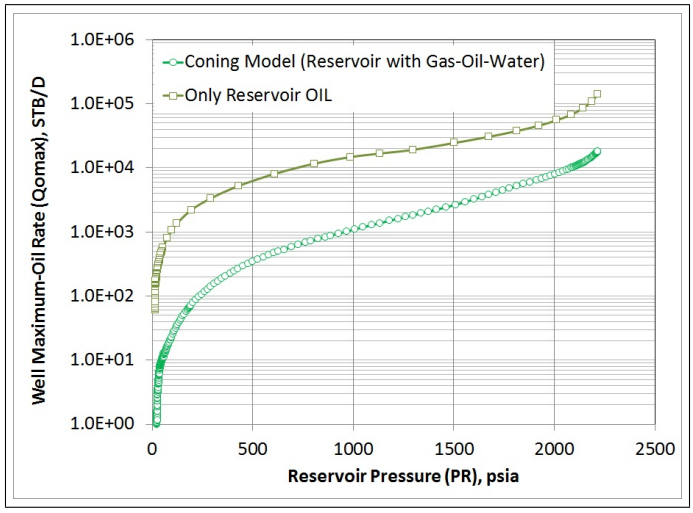

Figure 3.26: Coning Effect on Maximum Oil Rate.

Fig. 3.26 show the comparison of maximum oil rate between coning model and reservoir oil model. Reservoir oil model was generated from base case by isolating the oil zone from gas and water zone. The production comes from a horizontal well completed in the middle of oil zone. Both models were run with constant bottom-hole pressure of 10 psia to get the maximum oil rate. In Sensor, 10 psia is the minimum bottom-hole constraint value that we could use in the model. The oil production rate from the output file was recorded and plotted against reservoir pressure.

As predicted, the maximum oil rate from coning model is lower than the single phase reservoir oil model. We could see that there is a big reduction in maximum oil rate due to gas and water coning. If we plot the maximum oil rate versus reservoir pressure in a log-log scale, we could see that there is a different trend between both curves at the early stage of depletion. But at later stage, both curves show similar straight line trend.

Fig. 3.27 show the comparison of maximum gas rate between coning model and reservoir gas model. Reservoir gas model was generated from base case by isolating the gas zone from oil zone. The production comes from a horizontal well completed in the middle of gas column. The maximum gas rate for coning model is lower than reservoir gas model. From the log-log plot, we could see that there are different trends between two curves at the early stage of depletion and at the lower pressure, but the trend is similar in between.

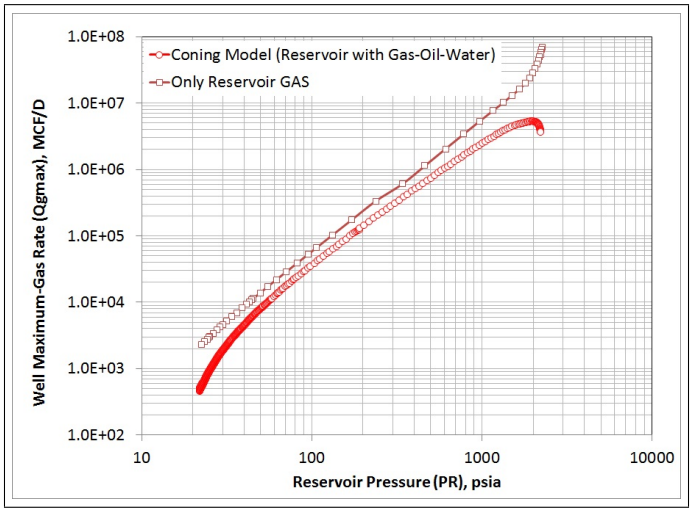

Figure 3.27: Coning Effect on Maximum Gas Rate.

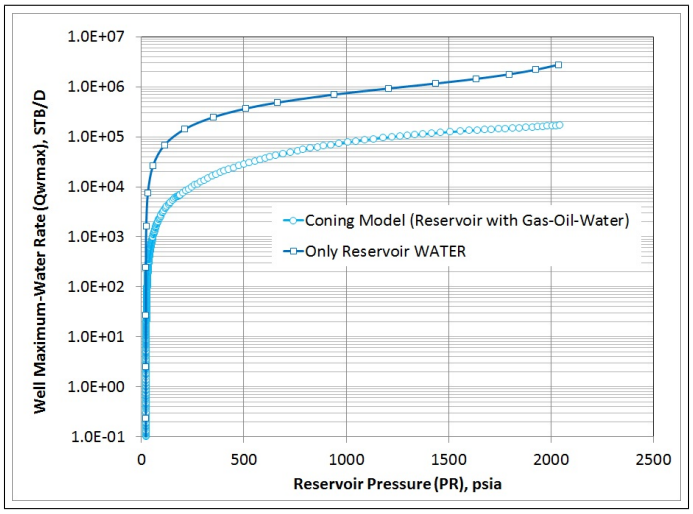

Figure 3.28: Coning Effect on Maximum Water Rate.

Fig. 3.28 show the comparison of maximum water rate between coning model and reservoir water model. Reservoir water model was generated from base case by isolating the water zone from oil zone. The production comes from one horizontal well completed in the middle of water column. The maximum water rate from reservoir water is higher than the coning model. From the log-log plot, we could see that there is different trend between two curves at early stage of depletion, but

in general, both have similar profile of maximum rate versus reservoir pressure. Based on this study, we could conclude that the maximum rate at coning condition is lower than the maximum rate at condition where production comes from single phase reservoir. The presences of other fluids in production stream that create a flow resistant is part of the reason. In coning model, where simultaneous gas and water coning occurs in thin oil reservoir, the maximum rate for each phase most likely depend on mobility, effective permeability, fluid density, gas cap size, aquifer size, and oil zone thickness.

Chapter 4

IPR MODELING FOR HORIZONTAL WELL WITH CONING

4.1 Introduction

Inflow Performance Relationship (IPR) is the relationship of well flowing bottomhole pressure (BHP) with well flow rate (q) at stabilized reservoir pressure. In many applications, IPR is used in production optimization. For examples; to determine tubing and choke size, adequate design of artificial lift, optimum well rate, production forecast, etc.

In 1935, Rawlins and Schellhardt [27] first present the concept of IPR by plotting the effect of liquid loading on production performance. Gilbert [15] is the first one who utilized curved which related flow rate with pressure and introduced them as IPR curves. In 1968, Vogel generated IPR curves for several hypothetical oil reservoirs with variety of PVT properties and relative permeability data by using a computer model. He also generated a dimensionless IPR for these set of IPR and proposed a relationship between the dimensionless parameters [31]. Since then, numbers of various correlations for IPR calculation have been proposed in literature.

Examples of IPR equations for horizontal well could be found in [9, 10, 17, 19, 20, 35]. The productivity equations can also be used to generate IPR. References 8,

23, and 27 present the productivity equations for horizontal well. These equations require several reservoir properties in its calculation (e.g permeability, reservoir thickness, etc).

In this study, based on the work of Vogel, we generated the IPR curves and its dimensionless form at any stage of depletion using Sensor black-oil simulator results. The IPR was generated for horizontal well with gas and water coning problems, producing from thin oil reservoir sandwiched between gas cap and aquifer. The IPR equation based on SPE paper by Whitson [33] that best-fit the gas, oil, water IPR is also presented in this study.

The empirical IPR generated with several major simplifying assumptions as follow: (1) The porous medium with areal permeability isotropy and vertical anisotropy; (2) Zero capillary pressure; (3) Skin effect is neglected; (4) Negligible frictional losses in horizontal wellbore; (5) The well is fully penetrating the reservoir in horizontal direction; (6) Reservoir model is run with initial pressure equal to bubble point.

4.2 Dimensional IPR Curves

Dimensional IPR curve was generated from pairs of flowing bottom-hole pressure and production rate at constant reservoir pressure. To represent the stage of depletion; instead of using recovery factor, we use reservoir pressure as a fraction of initial reservoir pressure. Since we modeled a three-phase reservoir, there will be an IPR curve each for gas, oil, and water phase.

The base case model was run with constant flowing bottom-hole pressure using Sensor simulator. The gas, oil, and water production rate and reservoir pressure from the output file were tabulated in an excel worksheet for further data processing. Repetition of the same procedure with different flowing bottom-hole pressure constraint was done to obtain more IPR data. An example of tabulated IPR data from the output file before sorting is shown in **Table 4.1**.

Since IPR curve is generated at constant reservoir pressure while the data are tabulated for each flowing bottom-hole pressure, a look-up and interpolation procedures in Excel are needed to get flowing bottom-hole and production data tabulated for constant reservoir pressure. The following is the excel function used to do interpolation and look-up [4]:

=FORECAST(NewX, OFFSET(KnownY, MATCH(NewX, KnownX, 1) – 1, 0, 2), OFFSET(KnownX, MATCH(NewX, KnownX, 1) – 1, 0, 2)

Table 4.1: Tabulated IPR Data from the Output File (Raw).

$P_{Ri} = 2291$ psia Remarks	P_{wf} psia	t days	P_R psia	q_g MCF/day	q_o STB/day	q_w days (STB/day)
$P_{wf} = 0.95\ P_{Ri}$	2176	0.5	2308.2	6695.7	14188.2	4839.3
	2176	0.7	2307.9	5814.0	12300.0	9655.9
	2176	0.8	2307.6	5042.3	10718.1	14101.3
	2176	1.1	2307.1	4449.1	9479.6	18165.3
	2176	1.5	2306.3	3989.8	8511.0	21887.7
	2176	2.1	2305.5	3615.4	7717.9	24339.4
	2176	2.8	2304.7	3363.8	7180.3	25686.3
	2176	3.5	2304.1	3260.2	6939.0	26267.6
	2176	4.0	2303.7	3225.7	6843.3	26555.1
	2176	4.5	2303.4	3213.9	6810.7	26674.8
	2176	4.9	2303.2	3210.0	6800.1	26697.9
	...	...	...	...	...	...
	...	...	...	...	...	...

This formula consists of 3 functions: (1) the FORECAST function to calculate the linear interpolation; (2) two calls to the MATCH function to search for a specified item in a range of cells, and then return the relative position of that item in the range; (3) two calls to the OFFSET function to returns a reference to a range that is specified number of rows and columns from a cell or range of cells [5]. It should be noted that the function above could be implemented directly in Excel provided the tabulated value are monotonic in x, which is the x-values are sorted. An example of sorted IPR data could be seen in **Table 4.2**. This function could be used by copying the formula into Excel and replacing $KnownX$ and $KnownY$ with the cell reference for the tabulate x and y values and $NewX$ with the x-value to interpolate. **Table 4.3** show the example of tabulated IPR data at $P_R = 0.95\ P_{Ri}$ after look-up and interpolation procedures.

Once the data completely tabulated for each reservoir pressure or depletion stage, the dimensional IPR curve could be generated by plotting flowing bottom-hole pressure versus production rate. This curve is a visual aid to observe the pressure-production behavior of individual well. Three dimensional IPR - each for gas, oil, and water phase for a horizontal well produce from thin oil zone sandwiched between gas cap and aquifer will be presented below.

Dimensional IPR for oil phase is presented in **Fig. 4.1**. The curves are parabolic and decline with decreasing reservoir pressure (P_R). It was found that there are different curve trends for different depletion stage. We also noticed at $P_R > 0.75\ P_{Ri}$,

Table 4.2: Tabulated Data from the Output File (Sorted). Here $P_{Ri} = 2291$ psia while $P_{wf} = 0.95\ P_{Ri}$.

P_{ro}	P_{wf}	t	q_g	q_o	q_w
psia	psia	days	MCF/day	STB/day	days (STB/day)
2183.5	2176	3650.0	17.9	39.4	0.0
2183.5	2176	3626.4	18.2	40.2	0.0
2183.5	2176	3573.0	18.7	41.1	0.0
2183.5	2176	3523.5	19.2	42.4	0.1
2183.5	2176	3465.5	19.7	43.3	0.1
2183.5	2176	3405.5	20.3	44.7	0.4
2183.5	2176	3345.5	20.7	45.5	0.6
2183.5	2176	3285.5	21.2	46.6	2.2
2183.5	2176	3213.9	21.6	47.7	4.7
2183.5	2176	3153.9	22.1	48.6	7.1
...	...	...	...	...	...
...	...	...	...	...	...

the oil productivity decrease rapidly with decreasing reservoir pressure; this might represent the effect of gas and water coning. After gas and water breakthrough, oil flow into the well is reduced significantly by gas and water coning.

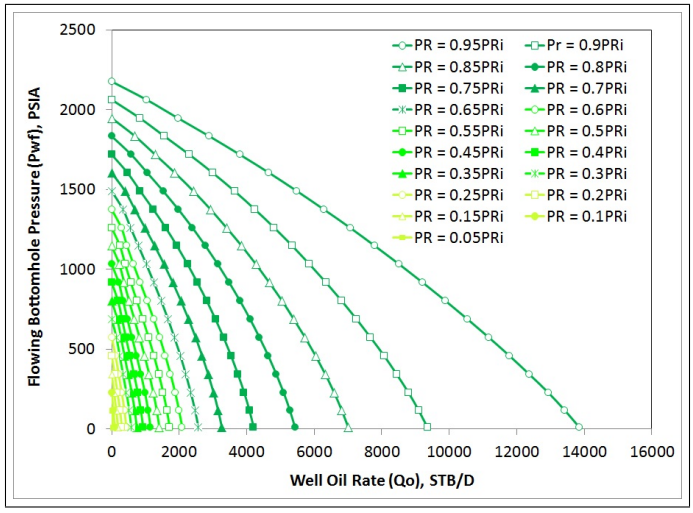

Figure 4.1: Dimensional IPR for Oil Phase.

In general, the productivity of horizontal well with gas and water coning will decreases as depletion proceeds. The reason could be decreasing reservoir pressure and increasing gas and water saturation due to coning that increase flow resistance

Table 4.3: Tabulated IPR Data after Look-Up and Interpolation.

P_R	2176	psia
$q_{g,max}$	4505555	MCF/day
$q_{o,max}$	13855	STB/day
$q_{w,max}$	199997	STB/day

P_{wf}	t	q_g	q_o	q_w
psia	days	MCF/day	STB/day	days (STB/day)
2176		0	0	0
2062	72.3	347299	1033	14780
1947	44.2	697812	1962	29293
1833	32.4	1017453	2896	42190
1718	25.6	1322947	3798	54535
1604	21.2	1610616	4663	66352
1489	18.1	1890813	5494	77922
1375	15.8	2156349	6285	89127
1260	14.0	2413833	7064	100118
1146	12.7	2659595	7799	110672
1031	11.5	2897362	8521	121257
916	10.6	3124056	9219	131621
802	9.8	3337843	9891	141617
687	9.1	3542635	10544	151362
573	8.5	3735066	11173	160638
458	8.0	3916408	11785	169747
344	7.6	4086757	12362	178202
229	7.2	4246168	12929	186137
115	6.9	4388019	13428	193712
10	6.6	4505555	13855	199997

to oil. For a constant flowing bottom-hole pressure (P_{wf}), there will be higher oil rate in high-pressure reservoir compare to low-pressure reservoir (**Fig. 4.1**). This primarily because higher reservoir pressure will result in higher well-drawdown for a constant P_{wf}; theoretically, oil rate is proportional with well-drawdown.

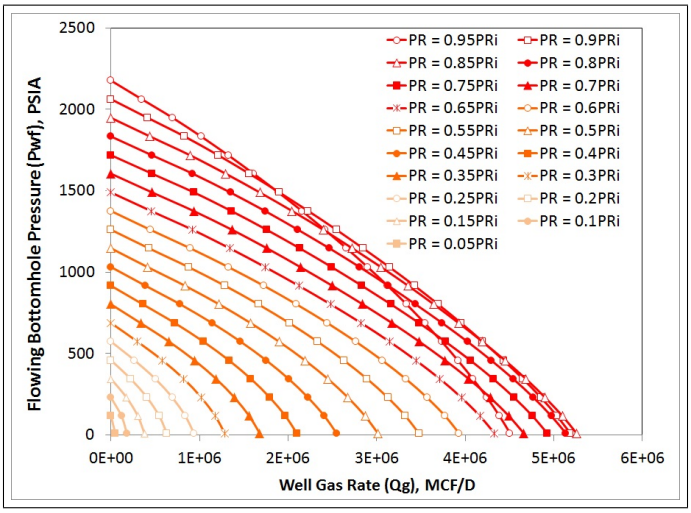

Figure 4.2: Dimensional IPR for Gas Phase.

Fig. 4.2 show the dimensional IPR for gas phase. This is the visual representation of pressure-gas production behavior of a horizontal well from the base case model. The gas production (well gas rate) mainly comes from the coning free-gas from gas cap; only relatively small fraction of production comes from the solution gas. As shown in **Fig. 4.2**, the IPR curves also have a curvature shape with quite similar trends when reservoir pressure goes below 0.85 P_{Ri}.

Different curves characteristic was found at early stage of depletion, when $P_R \geq 0.85\ P_{Ri}$. For detail observation, only three IPR curves at early stage of depletion were plot in **Fig. 4.3**. These curves might represent the gas coning development at early stage of depletion. When the well start producing above the critical rate, where the well drawdown causes viscous forces overcome the gravity forces, gas coning from gas cap will occurs. With decreasing reservoir pressure, the gas cap starts to expand and push the oil column down to the water zone (**Fig. 2.5**). This cause the gas-oil contact move closer to perforation point and results in severe gas coning where more gas produce in production stream. In this situation, as we observed in **Fig. 4.3**, the gas rate might increase with decreasing reservoir pressure.

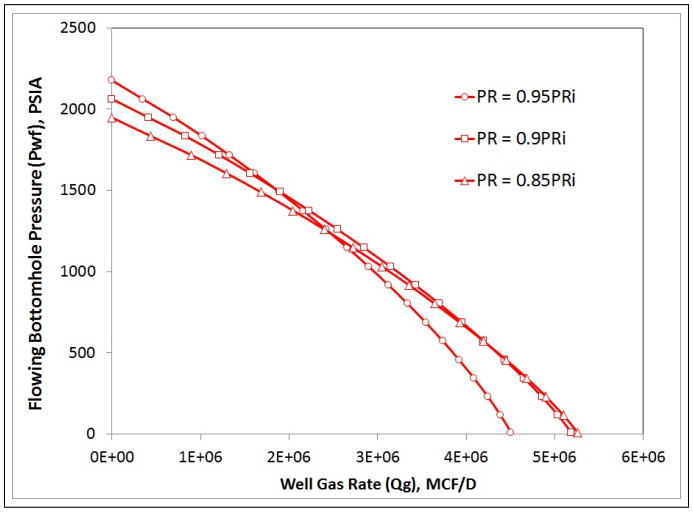

Figure 4.3: Dimensional IPR for Gas Phase (Early stage of depletion).

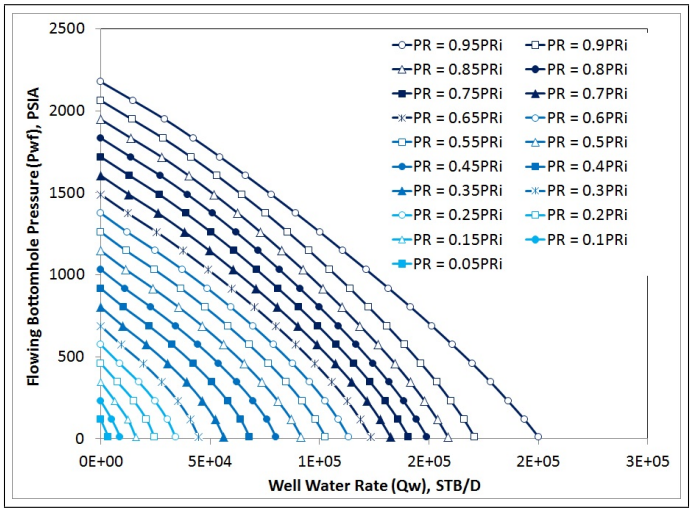

Figure 4.4: Dimensional IPR for Water Phase.

Dimensional IPR for water phase is presented in **Fig. 4.4**. This plot represents the pressure-water production behavior of horizontal well producing under three-phase flow condition. It should be noted that the water production comes from aquifer-water that cone into the well when the rate higher than critical rate.

The IPR curves are parabolic and decline with decreasing reservoir pressure (P_R). In general, the productivity will decreases as depletion proceeds. But refer

to **Fig. 4.4**, we observed that the water productivity decease quite rapid when the reservoir pressure goes from 0.95 P_{Ri} to 0.85 P_{Ri}, the curves trends are then similar until 0.5 P_{Ri} and somewhat slightly differ when reservoir pressure goes below 0.5 P_{Ri}. This curves characteristic might be caused by gas and water coning dynamic in reservoir. When the reservoir pressure decrease at early stage of depletion; gas cap start to expand and push the oil column to the water zone, the gas coning also start to build and dominate the flow in production stream. The combination of these event cause a higher resistance to water to flow and results in quite rapid decrease of water productivity at early stage.

4.3 Dimensionless IPR

In his work, Vogel also introduced the concept of dimensionless inflow performance relationship curves. He found that these dimensionless IPRs were remarkably similar throughout most of the producing life of the reservoir, thus it useful to utilize this curve in PI approximation for the typical well and reservoir. Dimensionless IPR is constructed by dividing the pressure of each point on an IPR curve by the maximum or shut-in pressure for that particular curve, and dividing the corresponding production rate by the maximum (100% drawdown) rate for the same curve [31]. The dimensionless IPR for each phase that was generated in this study is shown in **Fig. 4.5**, **Fig. 4.7**, and **Fig. 4.9**.

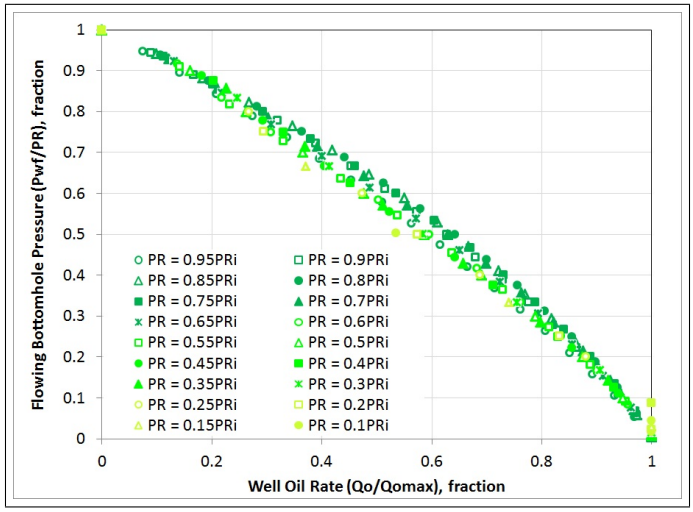

Figure 4.5: Dimensionless IPR for Oil Phase.

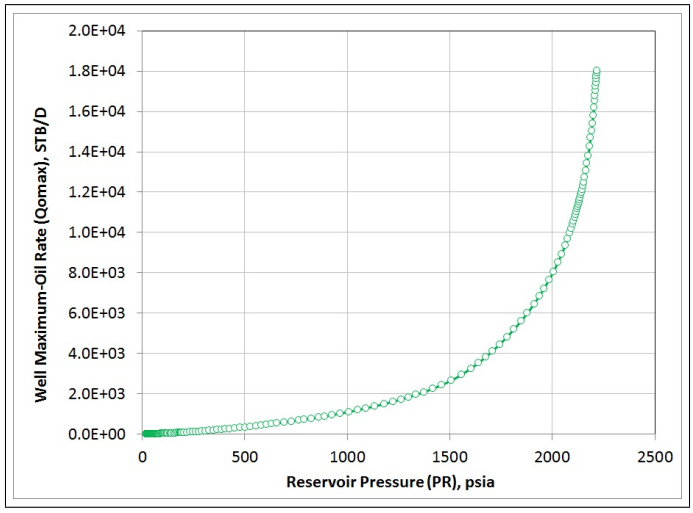

Figure 4.6: Maximum Oil Rate versus Reservoir Pressure.

To utilize the dimensionless curves, current reservoir pressure and maximum flow-rate data will be needed. While the current reservoir pressure is commonly measured, the maximum flow rate data is calculated using a correlation/approach which requires a flow test to implement. Thus, for practical purposes, we provide the plot of maximum open-flow rate versus reservoir pressure so that the maximum flow-rate could be found for known reservoir pressure. It should be noted that this plot was generated based on numerical simulation results. The base case model was run with the minimum bottom-hole constraint that allowed by Sensor simulator, the rate for each phase was then recorded as the maximum flow-rate and plotted against reservoir pressure (**Fig. 4.6**, **Fig. 4.8**, **Fig. 4.10**).

Dimensionless IPR for oil phase could be found in **Fig. 4.5**. Though the data appear to fit within a reasonable band, the trends seem to be affected by depletion. Bendakhalia and Aziz [9] observed that the curves trends which represent by depletion coefficient is not monotonic, but decrease as depletion proceeds and then slightly increase after reaching a minimum. Further discussion for this topic will be presented in Chapter 4.4.

The maximum oil rate as a function of reservoir pressure is shown in **Fig. 4.6**. The maximum oil rate is proportional with the reservoir pressure. Above 1500 psia, decreasing reservoir pressure will results in rapid decrease of maximum oil rate, while the change of maximum oil rate with pressure is less rapid for pressure below 1500 psia. In a well with constant P_{wf} constraint, the tendency of gas and

water coning is greater at high reservoir pressure (high drawdown) and lower at low reservoir pressure (low drawdown).

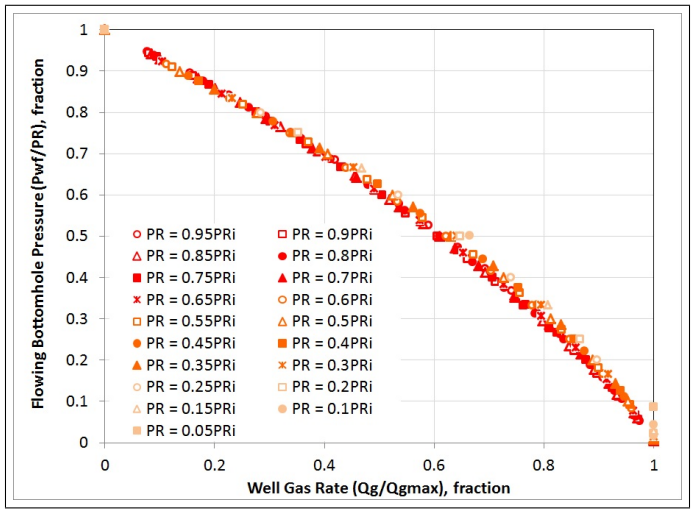

Figure 4.7: Dimensionless IPR for Gas Phase.

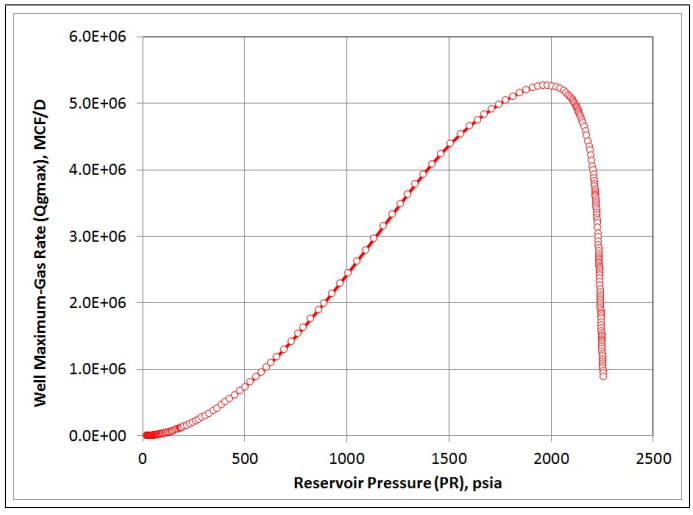

Figure 4.8: Maximum Gas Rate versus Reservoir Pressure.

Fig. 4.7 is the dimensional IPR for gas phase. We note that the data falls within a narrow range with an excellent correlation of the dimensionless trends. The maximum gas rate as a function of reservoir pressure is presented in **Fig. 4.8**. It was observed that gas production increase after reservoir start producing, this is

due to gas coning that occurs when dynamic force greater than gravitational force. But as depletion proceeds and a lower drawdown exist, the gas coning tendency and production rate is lower.

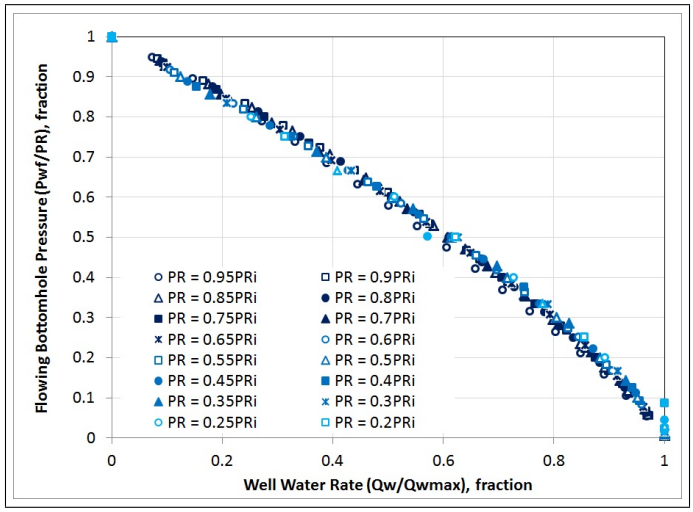

Figure 4.9: Dimensionless IPR for Water Phase.

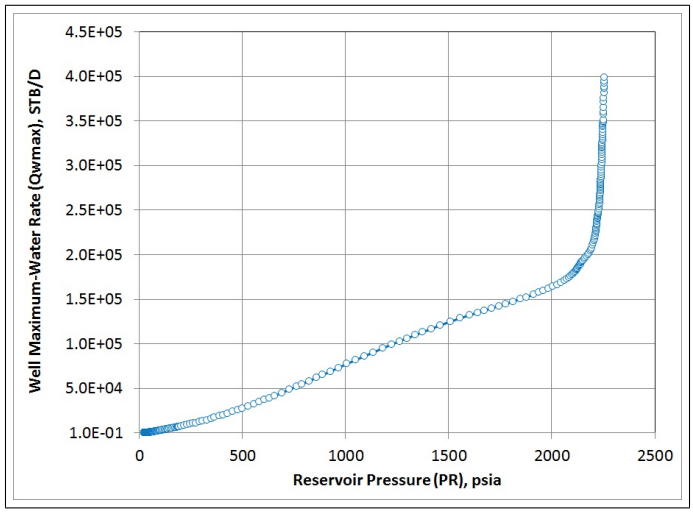

Figure 4.10: Maximum Water Rate versus Reservoir Pressure.

Dimensionless IPR for water phase is shown in **Fig. 4.9**. Similar with gas phase, we note that the data falls within a narrow range with an excellent correlation of the dimensionless trends. The maximum water rate is proportional with

reservoir pressure (**Fig. 4.10**). Since the well completed 5 ft from WOC, early water coning occurs when reservoir start producing. But as gas production from coning increase and dominate the flow, water production rate decrease rapidly. As depletion proceeds and the lower drawdown exist, the tendency of water coning and production rate is lower. Though the dimensionless IPR for gas and water phase appear to be independent from depletion stage, two generalized IPRs will still developed in this study for application purposes. The first empirical IPR will be developed as a function of reservoir pressure or depletion stage while the second empirical IPR will be developed based on all the generated data.

4.4 IPR Equation to Best-Fit Gas, Oil, and Water Phases

The formulation to best-fit the dimensionless IPR will be taken from IPR model presented by Whitson in SPE paper 12518 [33]. Whitson proposed a simple approach for OIL reservoir based on Fetkovich [14] suggestion that $F(P)$ for oil system can be approximated by two straight line joined at bubble point. Using the linear relationship of $F(P)$ as suggested by Fetkovich, Whitson defined the expression for dimensionless pseudo-pressure, m_d, for completely saturated system ($P_{wf} \leq P_R \leq P_b$) as:

$$m_d = 1 - V\left(\frac{P_{wf}}{P_R}\right) - (1 - V)\left(\frac{P_{wf}}{P_R}\right)^2 \tag{4.1}$$

Where

$$V = \frac{2x}{(x+1)} \tag{4.2}$$

Since we are using the assumption of negligible High Velocity Fluid (HVF) effect:

$$m_d = \frac{q}{q_{max}} \tag{4.3}$$

Hence, (4.1) becomes:

$$\frac{q}{q_{max}} = 1 - V\left(\frac{P_{wf}}{P_R}\right) - (1 - V)\left(\frac{P_{wf}}{P_R}\right)^2 \tag{4.4}$$

The formulation given by (4.4) will be used to best-fit the IPR models for gas, oil, and water phase in this study. This formulation is similar with the general IPR model proposed by Richardson and Shaw for solution gas reservoirs [28].

4.4.1 Depletion based IPR

Since the pressure-production rate behavior of a horizontal well appears to be affected by depletion [9], an empirical IPR was developed based on simulated data on each reservoir pressure (stage of depletion). The equations used to best-fit the IPR model for each phase are:

$$\textbf{Oil phase}: \quad \frac{q_o}{q_{o,max}} = 1 - V_o\left(\frac{P_{wf}}{P_R}\right) - (1 - V_o)\left(\frac{P_{wf}}{P_R}\right)^2 \tag{4.5}$$

$$\textbf{Gas phase}: \quad \frac{q_g}{q_{g,max}} = 1 - V_g\left(\frac{P_{wf}}{P_R}\right) - (1 - V_g)\left(\frac{P_{wf}}{P_R}\right)^2 \tag{4.6}$$

$$\textbf{Water phase}: \quad \frac{q_w}{q_{w,max}} = 1 - V_w\left(\frac{P_{wf}}{P_R}\right) - (1 - V_w)\left(\frac{P_{wf}}{P_R}\right)^2 \tag{4.7}$$

Where V_o, V_g, and V_w is the parameter in general quadratic equation for oil, gas, and water. Bendakhalia and Aziz observed that V is a function of reservoir recovery or depletion, thus they defined V as the depletion coefficient.

The following are procedures to calculate V_o, V_g, and V_w at each reservoir pressure:

1. Assume V_o, V_g, and V_w value as initial guess. The value should between 0 and 1.
2. Calculate P_{wf}/P_R for each data point.
3. For each phase, calculate the analytical $\frac{q}{q_{max}}$ by using (4.5)-(4.7).
4. Calculate the error square between numerical and analytical $\frac{q}{q_{max}}$ using equation below

$$\frac{q}{q_{max}} = \left[\frac{(q/q_{max})_{\text{analytical}} - (q/q_{max})_{\text{numerical}}}{(q/q_{max})_{\text{numerical}}}\right]^2 \tag{4.8}$$

5. Calculate the Sum of Square Error for gas, oil, and water ($\text{SSQ}_g, \text{SSQ}_o$, and SSQ_w)

6. Calculate the Total SSQ;

$$\text{Total SSQ} = \text{SSQ}_g + \text{SSQ}_o + \text{SSQ}_w \tag{4.9}$$

7. Utilize SOLVER in MS Excel to minimize the Total SSQ by changing V_o, V_g, and V_w values.

The procedures above were repeated for all reservoir pressure. **Fig. 4.11** presents the V_o and SSQ_o values for the ranges of reservoir pressure studied. The SSQ_o was also plotted to observe how fit the data with the IPR model.

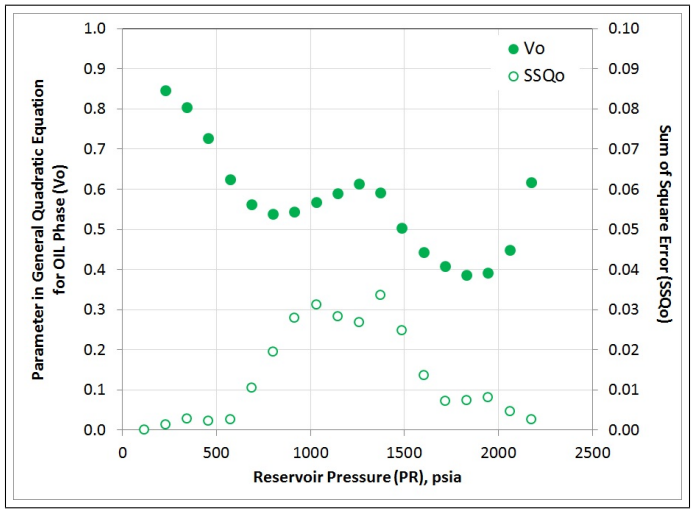

Figure 4.11: V_o and SSQo as a Function of Reservoir Pressure.

From **Fig. 4.11**, we note that V_o, or depletion coefficient for oil phase as defined by Bendakhalia and Aziz, is not monotonic. The SSQ_o curve is higher at reservoir pressure between 750 – 1500 psia, this indicate an increasing lack of fit of the data on this region. We would comment that the V_o points in higher SSQ_o region are located out of the trend, thus it is possible that these data points actually following the trend of other data points. It appears that Vo decreases with decreasing reservoir pressure and then increase after some point. Similar observation of depletion coefficient for oil phase was made by Bendakhalia-Aziz ([9]) and Wiggins-Wang ([35]).

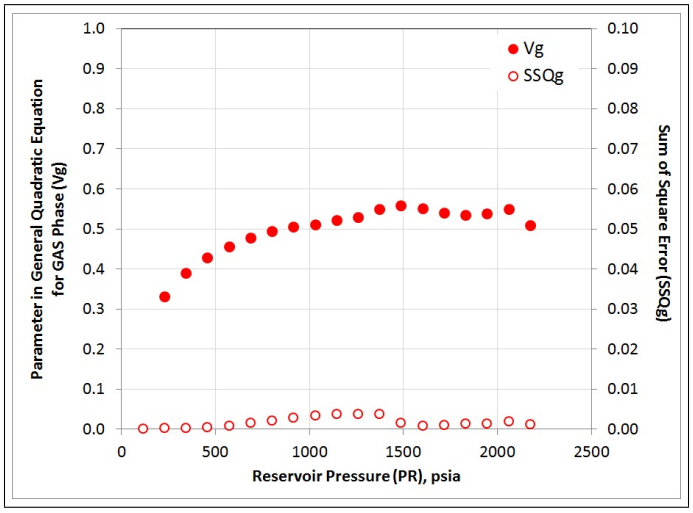

Figure 4.12: V_g and SSQg as a Function of Reservoir Pressure.

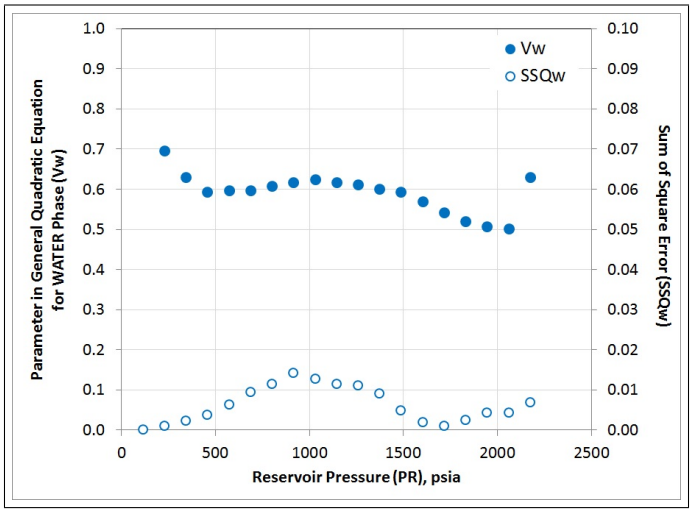

Figure 4.13: V_w and SSQw as a Function of Reservoir Pressure.

Fig. 4.12 show the relation between V_g with reservoir pressure. In general, the V_g value decrease with decreasing reservoir pressure within value range of 0.3 – 0.6. An excellent fit of the data with the IPR model is represented by a low SSQ_g values throughout the depletion stage. For water phase, the V_w values lay within the range of 0.5 – 0.7 with maximum SSQ_w of 0.015 (**Fig. 4.13**).

Table 4.4: Summary of V and SSQ Values for Generalized IPR.

Parameter in General Quadratic Equation	Value	SSQ	Value
V_o	0.522	SSQ_o	0.565
V_g	0.526	SSQ_g	0.063
V_w	0.576	SSQ_w	0.189

Compare to oil phase, the empirical IPR show a better fit for gas and water phase. Thus, a better estimate of gas and water performance should be expected in its application. We also noted that the depletion coefficient (V) is not monotonic, and there are different trends of depletion coefficient for each phase. This non-monotonic behavior might indicate that the IPR is independent (or only a weak function) of depletion stage. It should be noted that further studies will be needed to validate this conclusion.

4.4.2 Generalized IPR

The second empirical IPR for each phase was developed based on all generated data. Considering that the data appear to fit within reasonable band and there is an indication that the IPR is independent of depletion, the generalized IPR might accurate enough to estimate the three-phase inflow performance of horizontal well produce from thin oil column sandwiched between gas cap and aquifer. This suggestion is supported by Wiggins and Wang observation that the depletion based IPR provide no better results than the generalized IPR.

The generalized IPR was developed using the same procedures as depletion based IPR. But instead of calculating the SSQ for each reservoir pressure, the SSQ was calculated for all data. Thus there are only three V values for all data, each for gas, oil, and water phase. **Table 4.4** presents the V and SSQ values for generalized IPR.

As shown in **Table 4.4**; the calculation of V_g, V_o, and V_w results in approximately the same value of 0.5. Though this value might changes for different reservoir properties, it could not be overemphasize that V_g, V_o, and V_w values will approximately the same. Thus, it is possible to use one generalized IPR for gas, oil, and water phases with reasonable accuracy. Using (4.4) and the V values obtained in this study, the resulting generalized IPR for each phase could be wrote as follow:

$$\textbf{Oil phase}: \quad \frac{q_o}{q_{o,max}} = 1 - 0.522\left(\frac{P_{wf}}{P_R}\right) - 0.478\left(\frac{P_{wf}}{P_R}\right)^2 \tag{4.10}$$

$$\textbf{Gas phase}: \quad \frac{q_g}{q_{g,max}} = 1 - 0.526\left(\frac{P_{wf}}{P_R}\right) - 0.474\left(\frac{P_{wf}}{P_R}\right)^2 \tag{4.11}$$

$$\textbf{Water phase}: \quad \frac{q_w}{q_{w,max}} = 1 - 0.576\left(\frac{P_{wf}}{P_R}\right) - 0.424\left(\frac{P_{wf}}{P_R}\right)^2 \tag{4.12}$$

Based on the SSQ values, we noted that the generalized IPR give the best-fit for gas phase. The visual comparison between the generalized IPR curves with numerical data is presented in **Fig. 4.14** – **Fig. 4.16**.

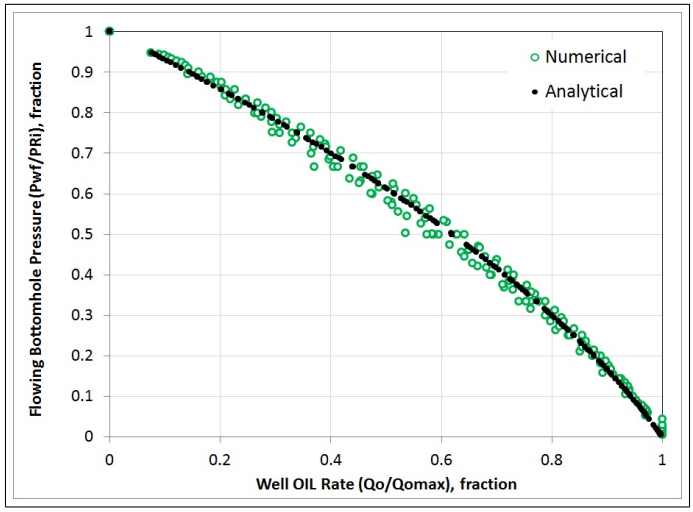

Figure 4.14: Comparison of Generalized IPR with Numerical Data for Oil Phase.

We noted a good correlation between numerical data with the proposed generalized IPR from **Fig. 4.14** – **Fig. 4.16**. For oil phase, the generalized IPR results in less than 5% error at high-medium reservoir pressure and around 15% error at low reservoir pressure. For gas and water phase, the error is around 3% at high-medium reservoir pressure and 10% at low reservoir pressure. The generalized IPR fit better for early stages than later stages of depletion. It appears that this

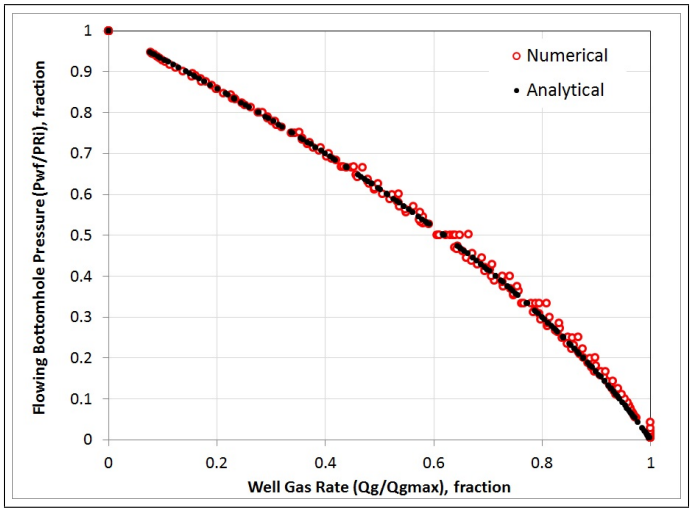

Figure 4.15: Comparison of Generalized IPR with Numerical Data for Gas Phase.

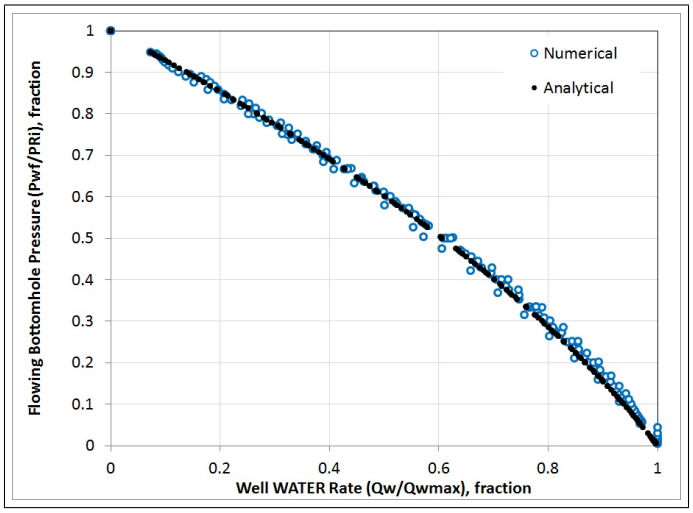

Figure 4.16: Comparison of Generalized IPR with Numerical Data for Water Phase.

lack of fit is increasing with increasing stages of depletion. Decreasing amount of simulated data available for analysis with increasing stages of depletion could be one of the reasons. However, the error of generalized IPR is least at early stages of depletion where the production is high and becomes higher at later stages where the production is low. Thus, the impact of this error to performance prediction is considered low.

Chapter 5

CONCLUSIONS

Inflow Performance Relationship of a horizontal well producing from thin oil zone sandwiched between gas cap and aquifer were developed based on reservoir simulator results. An additional sensitivity study was done to better understand the coning behavior in the model.

From this study, the following conclusions are presented:

1. For the same dataset, Sensor black oil model proved to run 10 times faster than Sensor compositional model. The simulation results from both model is in range of 5% differences.

2. The optimum grid numbers of 1480 ($N_x = 40$, $N_y = 1$, $N_z = 37$) with a converged solution was obtained from grid sensitivity study.

3. Default Implicit solver in Sensor (ILU 011) giving the least CPU time for our particular problem.

4. Higher horizontal permeability results in higher recovery and delayed gas and water coning. In a reservoir with high horizontal permeability, the fluids will tend to flow in horizontal direction than vertical direction. This will reduce the tendency of gas and water to cone into the well.

5. In high horizontal permeability reservoir ($k_h = 1000$ mD), vertical anisotropy ratio only has slight effect on gas coning. But increase of k_v/k_h value will result in higher water cut when breakthrough happen, the water cut will decrease (faster) when k_v/k_h increase. In high horizontal permeability reservoir ($k_h = 300$ mD), higher vertical anisotropy ratio will results in early gas

breakthrough but slower increase of GOR; vertical anisotropy ratio only has slight effect on water coning.

6. Gas cap size does not affect the water and gas breakthrough time, but trends of GOR and water cut after breakthrough is affected by gas cap size. Bigger gas cap size results in higher GOR but lower water cut. Increase in gas cap size will results in lower oil recovery factor.

7. Aquifer size does not affect the gas and water breakthrough time. Increase in aquifer size will leads to higher water cut and lower GOR. There is only slight effect of aquifer size on oil recovery; with tripled aquifer volume, the oil recovery increase less than 1%.

8. The trends of oil recovery with different well depth are changes with time; in a long production period, it appears to be beneficial to place horizontal well in upper section of the oil leg. It is recommended to generate the plot of oil recovery versus well depth based on particular reservoir, development plan, and well configuration data; and use it as a tool to help in deciding the optimum well placement.

9. When the horizontal well completed below WOC, 'inverse coning' of oil to the well will happen in early period. But when the gas pushes oil column to the water zone, the well actually produces from an oil column with gas and water coning. So the inverse coning contributes in oil recovery at early period, but the oil recovery at later stage relies on gas from gas cap that pushes the oil into water zone.

10. A relationship curve between reservoir pressures and flowing bottom-hole pressure when the cone collapse was presented in this study. The ratio of bottom-hole pressure to reservoir pressure at which the cone starts to collapse is higher for water coning than gas coning. This means, compare to gas cone collapse, higher bottom-hole pressure will be needed to make the water cone collapse.

11. The maximum rate at coning condition is lower than the maximum rate at condition where production comes from single phase reservoir.

12. Three dimensional IPR for our particular model - each for gas, oil, and water phase were generated in this study. These curves could help in observing

the pressure-production behavior of individual well. In general, the productivity of horizontal well with gas and water coning will decreases as depletion proceeds.

13. Dimensionless IPR and maximum rate as a function of reservoir pressure for each phase is presented in this study. We noted that the data falls within a narrow range with an excellent correlation of the dimensionless trends.

14. Two empirical IPR, depletion based IPR and generalized IPR, were developed based on formulation given by Whitson.

15. From depletion based IPRs, we observed that the depletion coefficient (V) is not monotonic, and there are different trends of depletion coefficient for each phase. The non-monotonic behavior might indicate that the IPR is independent (or only a week function) of depletion stage.

16. Calculation of V_g, V_o, and V_w for the generalized IPR results in approximately the same value of 0.5. Though this value might changes for different reservoir properties, we suggest that the V_g, V_o, and V_w values will approximately the same.

Nomenclatures

B_g	=	gas formation volume factor
B_o	=	oil formation volume factor
N_x	=	number of grids in x-direction
N_y	=	number of grids in y-direction
N_z	=	number of grids in z-direction
NZTOP	=	number of cells in z-direction; above the well
NZBOTTOM	=	number of cells in z-direction; below the well
P_{wf}	=	flowing bottom-hole pressure, bara or psia
P_R	=	reservoir pressure, bara or psia
q	=	production rate, STB/D
q_{max}	=	maximum production rate, STB/D
R_x	=	$\Delta x_{i+1}/\Delta x_i$
R_z	=	$\Delta z_{i+1}/\Delta z_i$
SSQ_o	=	Sum of Square of Error for oil phase
SSQ_g	=	Sum of Square of Error for gas phase
SSQ_w	=	Sum of Square of Error for water phase
V_o	=	parameter in general quadratic IPR equation for oil phase
V_g	=	parameter in general quadratic IPR equation for gas phase
V_w	=	parameter in general quadratic IPR equation for water phase
Δx	=	grid size in block-i
Δy	=	grid size in block-j
Δz	=	grid size in block-k

Bibliography

[1] http://www.coatsengineering.com

[2] http://petrostreamz.com/pipe-it

[3] Sensor Manual

[4] http://www.blueleafsoftware.com/Products/Dagra/LinearInterpolationExcel.php

[5] Excel Help and How-to

[6] Ahmad, T., Reservoir Engineering Handbook Third Edition, Gulf Professional Publishing, 2006.

[7] Appleyard, J. R. and Cheshire, I. M., Nested Factorization, SPE 12264 presented at the 7th SPE Symposium on Reservoir Simulation in San Francisco (November 1983).

[8] Babu, D. K. and Odeh, A. S., Productivity of a Horizontal Well, SPE Paper 18298 presented at the 1988 SPE Ann. Tech. Conf. and Exhibition Houston.

[9] Bendakhlia, H. and Aziz, K., Inflow Performance Relationships for Solution Gas Drive Horizontal Wells, SPE Paper 19823 presented at 64th SPE Annual Technical Conference and Exhibition, San Antonio Texas (October 1989).

[10] Billiter, T., Lee, J., Chase, R., Dimensionless Inflow-Performance-Relationship Curve for Unfractured Horizontal Gas Well, SPE Paper 72361 presented at SPE Eastern Regional Meeting, Canton Ohio (October 2001).

[11] Daviau, F. et al., Pressure Analysis for Horizontal Wells, SPE 14251 presented at SPE Annual Technical Conference and Exhibition, Las Vegas (September 1985).

[12] Eickmeier, J. R., How to Accurately Predict Future Well Productivities, World Oil (May 1968).

[13] Elgaghah, S. A. et al., A Simple Productivity Equation for Horizontal Wells Based on Drainage Area Concept, SPE 35713 presented at Western Regional Meeting in Alaska (May 1996).

[14] Fetkovich, M. K., The Isochronal Testing of Oil Wells, SPE Paper 529 presented at SPE Annual Meeting, Las Vegas (September 1973).

[15] Gilbert, W. E., Flowing and Gas Lift Well Performance, API Drilling and Production Practice, 1954, Dallas-Texas.

[16] Haug, B. T., Ferguson, W.I., Kydland, T., Horizontal Well in the Water Zone: The Most Effective Way for Tapping Oil from Oil Zones?, SPE 22929 presented at 66th Annual Technical Conference and Exhibition, Dallas Texas (October 1991).

[17] Huang, B. et al., A New IPRs Establishment and Solution for Horizontal Wells, SPE Paper 39570 presented at SPE India Oil and Gas Conference and Exhibition, New Delhi India (February 1998).

[18] Ibelegbu, C., Determination of Cone Receding Time in Horizontal Well, SPE 140684 presented at the 34th Annual SPE International Conference and Exhibition, Tinapa Nigeria (August 2010).

[19] Jabbari, H. and Economides, M. J., A New Approach to IPR Curves of Horizontal Wells in Two-Phase Reservoirs, SPE 115918 presented at SPE Annual Technical Conference and Exhibition, Colorado USA (September 2008).

[20] Kamkom, R. and Zhu, D., Evaluation of Two-Phase IPR Correlations for Horizontal Wells, SPE Paper 93986 presented at SPE Production and Operations Symposium, Oklahoma USA (April 2005).

[21] Karcher, B. J., Giger, F. M., and Combe, J., Some Practical Formulas to Predict Horizontal Wells Behavior, SPE Paper 15430 presented at the 1986 SPE Ann. Tech. Conf. and Exhibition New Orleans.

[22] Lee, R. L., et al., Water Cone Subsidence Time of a Horizontal Well, SPE 29295 presented at SPE Asia Pacific Oil and gas Conference, Kuala Lumpur Malaysia (March 1995).

[23] Mukherjee, H. and Economides, M. J., A Parametric Comparison of Horizontal and Vertical Well Performance, SPE Paper 18303 presented at the 1989 SPE Ann. Tech. Conf. and Exhibition San Antonio.

[24] Ozkan, E., Raghavan, R., and Joshi, S. D., Horizontal Well Pressure Analysis, SPEFE (December 1989).

[25] Papatzacos, P. et al. Cone Breakthrough Time for Horizontal Wells, SPE 19822 presented at the 64th SPE Annual Technical Conference and Exhibition, San Antonio-Texas (October 1989).

[26] Price, H. S. and Coats, K. H., Direct Methods in Reservoir Simulation, SPEJ, June 1974, Trans. AIME 257.

[27] Rawlins, E. L. and Schellhardt, M. A., Backpressure Data on Natural Gas Wells and Their Application to Production Practices, Monograph Series, USBM (1935).

[28] Richardson, J. M. and Shaw, A. H., Two-Rate IPR Testing a Practical Production Tool, JCPT (March April 1982).

[29] Uhri, D. C., and Blount, E. M., Pivot Point Method Quickly Predicts Well Performance, World Oil (May 1982).

[30] Vinsome, P. K. W., Orthomin, an Iterative Method for Solving Sparse Sets of Simultaneous Linear Equations, SPE 5729 presented at the SPE 4th Symposium of Numerical Reservoir Simulation in Los Angeles (February 1976).

[31] Vogel, J. V., Inflow Performance Relationships for Solution-Gas Drive Wells, JPT, January 1968

[32] Wagenhofer, T., and Hatzignatiou, D., G., Optimization of Horizontal Well Placement, SPE 35714 presented at Western Regional Meeting, Anchorage Alaska (May 1996).

[33] Whitson, C. H., Reservoir Well Performance and Predicting Deliverability, SPE Paper 12518 (1983).

[34] Whitson, C.H. and Torp, S.B. ,Evaluating Constant Volume Depletion Data, JPT, March 1983; Trans., AIME, 275.

[35] Wiggins, M. L. and Wang, H. S., A Two-Phase IPR for Horizontal Oil Wells, SPE 94302 presented at SPE Production and Operations Symposium, Oklahoma USA (April 2005).

Appendix

Sensor Input Data File for Base Case Model

```
TITLE

 IPR MODELING FOR CONING WELL

 "TROLL" OIL WELL - 3650 DAYS OF 1-WELL PRODUCING.

ENDTITLE

GRID   40 1 37

ILU 0 1 1

IMPLICIT

MAPSPRINT 1  P SAT SO SG SW DEPTH PSAT TENS

MAPSFILE P SAT SO SG SW
C MAPSPRINT 1  P PSAT SW SO SG PV H DEPTH TX TY TZ KZ ROCKTYPE GW GO GG

C      Bwi    cw    denw  visw  cf   pref
C     rb/stb 1/psi  #/ft3  cp  1/psi psia
MISC    1.   3E-6    63.   .5  5E-6  3550

KRANALYTICAL 1
 0.2  0.2  0.2  0.05    ! Swc  Sorw  Sorg  Sgc
 0.5  0.7  1.0          ! krw(Sorw)  krg(Swc)  kro(Swc)
 3  3  3  3             ! nw now ng nog
```

```
C ---------------------------------------------------------------------
C Grid dimensions - generated from Grid Builder Excel Sheet
C ---------------------------------------------------------------------

INCLUDE
DELX.inc

INCLUDE
DELY.inc

INCLUDE
DELZ.inc

C ---------------------------------------------------------------------

POROS CON
  .25
MOD
 1   40 1 1  1  1 = 100    ! BIG GAS CAP
 1   40 1 1 37 37 = 100    ! BIG AQUIFER

DEPTH CON
 5000

KX CON
  1000

KY EQUALS KX

KZ EQUALS KX
MOD
1 40  1 1  1 37 * 0.25

C ---------------------------------------------------------------------
C Automatic conversion of EOS to Black Oil Table
C ---------------------------------------------------------------------
```

```
C        ipvttype  nsat  ntot
BLACKOIL    1       15    15
 PRESSURES  14.7 100 250 500 750 1000 1250 1500 1750 2000 2100 2291 2500
2750 3000
 RESERVOIR FLUID
  0.00371018 0.40442424 0.04443788 0.01973696 0.22678725 0.20551770
  0.07982091 0.01556488
INJECTION GAS EQUILIBRIUM
 SEPARATOR
  14.7   60.
ENDBLACKOIL

C Include EOS
INCLUDE
 eos8x-viso14.inc

C ----------------------------------------------------------------------

INITIAL

C  depth psat
DEPTH  PSATBP
5050.  2291.

C PINIT 2291 - DO NOT enter PINIT if GOC is entered
GOC   5050
HWC   5100

ENDINIT

WELL
     I J K
  PROD1
    1  -1  26
```

```
WELLTYPE
 PROD1  RBTOT

BHP
 PROD1  1500

MAPSFREQ 1
MAPSFILEFREQ 1

RATE
 PROD1  10000

TIME 7300 365

END
```